SLC2A1 plays a significant prognostic role in lung adenocarcinoma and is associated with tumor immunity based on bioinformatics analysis

Yuhang Wang[1#^], Hui Wen[1#], Daqiang Sun[1,2]

[1]Graduate School, Tianjin Medical University, Tianjin, China; [2]Department of Thoracic Surgery, Tianjin Chest Hospital of Tianjin University, Tianjin, China

Contributions: (I) Conception and design: Y Wang; (II) Administrative support: D Sun; (III) Collection and assembly of data: H Wen; (IV) Data analysis and interpretation: Y Wang; (V) Manuscript writing: All authors; (VI) Final approval of manuscript: All authors.

[#]These authors contributed equally to this work.

Correspondence to: Daqiang Sun. Department of Thoracic Surgery, Tianjin Chest Hospital of Tianjin University, No. 261, Taierzhuang South Road, Jinnan District, Tianjin 300222, China. Email: sdqmd@163.com.

Background: The treatment of lung adenocarcinoma (LUAD) has been stuck in a bottleneck due to a number of factors. There is a pressing need for research into potential genetic markers to help drug development and improve the prognosis of patients. *SLC2A1* has been reported in multiple LUAD-related prognosis prediction signatures. However, the role of *SLC2A1* in the occurrence and development of LUAD and its impact on prognosis remain elusive.

Methods: The Cancer Genome Atlas (TCGA) and Gene Expression Omnibus (GEO) were used to acquire the samples. We used R to perform statistical analysis, Gene Set Enrichment Analysis (GSEA), immune infiltration and immune cell correlation analysis, drug sensitivity analysis, and visualization. The immune cell score was calculated using the Timer2.0 database. Prognostic analysis was performed using R, Gene Expression Profiling Interactive Analysis (GEPIA), and the Kaplan-Meier Plotter. Overall survival and progression free survival were the main outcome of prognosis analysis. Protein-protein interaction, disease-genetics analysis, and tissue-specific enrichment analyses were performed using Metascape.

Results: *SLC2A1* was highly expressed in LUAD tissues. Univariate COX regression [hazard ratio (HR) =1.689, 95% confidence interval (CI): 1.242–2.249, P<0.001] and multivariate COX regression including age, gender, smoking, TNM stage and SLC2A1 expression (HR =1.567, 95% CI: 1.127–2.179, P=0.008) showed that *SLC2A1* was an independent prognostic risk factor for LUAD. GSEA and Metascape analysis showed that *SLC2A1* was strongly associated with the cell cycle, mitosis, lung tissue, and tumor recurrence. Immune correlation analysis showed that SLC2A1 was associated with two tumor infiltration immune cells: activated CD (cluster of differentiation)4$^+$ memory T cells (r=0.31, P=0.003) and activated mast cells (r=–0.28, P=0.010). Moreover, patients with high *SLC2A1* expression had higher immune checkpoint molecules and Tumor Immune Dysfunction and Exclusion (TIDE) scores, indicating poorer immunotherapy efficacy. Patients with high *SLC2A1* expression were more sensitive to chemotherapy drugs and less sensitive to targeted drugs compared to those with low *SLC2A1* expression.

Conclusions: The high expression of *SLC2A1* in LUAD predicted poor prognosis and was closely related to tumor immunity, which could be used as an effective prognostic biomarker to provide a new strategy for clinical prognosis assessment and immunotherapy for LUAD.

Keywords: SLC2A1; lung adenocarcinoma (LUAD); prognosis; tumor-infiltrating immune cells (TIICs); immunotherapy

^ ORCID: 0000-0002-7457-5718.

Submitted Feb 11, 2022. Accepted for publication Apr 02, 2022.
doi: 10.21037/atm-22-1430
View this article at: https://dx.doi.org/10.21037/atm-22-1430

Introduction

Lung cancer remains the leading cause of cancer-related death worldwide, with an estimated 5-year relative survival rate of 21% in 2021 (1). Lung adenocarcinoma (LUAD) is the most common pathological subtype of lung cancer, accounting for 40% of lung cancer cases (2). In recent years, with the development of targeted therapy and immunotherapy, the treatment of LUAD has gradually entered the era of precision therapy (3,4). However, the treatment of LUAD has been stuck in a bottleneck due to a number of factors, such as the improvement of anti-tumor drug resistance (5,6). In addition to the currently known genetic biomarkers (such as driver genes), there are many undiscovered genetic changes that may play important roles in the occurrence and development of LUAD. Therefore, there is a pressing need for research into potential genetic markers to help drug development and improve the prognosis of patients.

Solute carrier (SLC) transporters are a family of more than 300 membrane-bound proteins that play an important role in the absorption of various nutrients and drugs by cells (7). *SLC2A1* is a member of the SLC transporter family, which has been reported in multiple LUAD-related prognosis prediction signatures (8-10). Recent study (11) has shown that SLC2A1 has prognostic significance in patients with LUAD after surgical resection. However, as a single gene, the role of *SLC2A1* in the occurrence and development of LUAD and its impact on prognosis remain elusive. As more and more attention has been paid to the role of tumor immune microenvironment and tumor immune infiltrating cells (TIICs), the role of *SLC2A1* in lung adenocarcinoma tumor immunity is still unclear.

According to our previous studies, we found that the expression of *SLC2A1* was correlated with the prognosis of patients with LUAD. On this basis, we want to further explore the role of *SLC2A1* in the occurrence and development of and tumor immunity of LUAD based on bioinformatics methods, so as to provide new targets for molecular targeted therapy and immunotherapy of LUAD. We present the following article in accordance with the REMARK reporting checklist (available at https://atm.amegroups.com/article/view/10.21037/atm-22-1430/rc).

Methods

In this study, we explored the expression of *SLC2A1* in LUAD and its prognostic value in LUAD patients based on TCGA (The Cancer Genome Atlas) and GEO (Gene Expression Omnibus) databases. We analyzed the differential expression network of *SLC2A1* and the possible mechanism of its impact on the prognosis of LUAD through multi-dimensional analysis. We also analyzed the correlation between *SLC2A1* expression and tumor immune infiltration, as well as the role of *SLC2A1* in guiding immunotherapy decisions. Furthermore, the relationship between *SLC2A1* expression and the drug sensitivity of LUAD was also explored. Our study comprehensively verified the potential role of *SLC2A1* in LUAD, which may provide a new biomarker for the treatment and prognostic assessment of LUAD patients, and provide new suggestions for clinical decision-making. The study was conducted in accordance with the Declaration of Helsinki (as revised in 2013).

Data collection and pretreatment

The datasets used in the current research were acquired from TCGA (https://portal.gdc.cancer.gov/) and GEO (https://www.ncbi.nlm.nih.gov/geo/). The RNA (Ribonucleic Acid) sequencing FPKM (Fragments Per Kilobase of exon model per Million mapped fragments) data of 11,093 pan-cancer samples were downloaded from TCGA-ALL. The RNA sequencing counts data and FPKM data of 535 tumor samples of LUAD and the corresponding clinical information were downloaded from TCGA-LUAD. There were a total 486 tumor samples with complete information on age, gender, smoking, TNM (Tumor Node Metastasis) stage, vital status, and overall survival (OS) time.

Additionally, the microarray data of LUAD of four datasets [GSE118370 (n=12), GSE140797 (n=14), GSE32863 (n=116), GSE40275 (n=84)] were downloaded from the GEO database for validation. The extracted data were normalized and processed by log2 transformation, and the data were normalized using the "preprocessCore" package (12) in R software (version 4.1.0, Copyright (C) 2021 The R Foundation for Statistical Computing). The

Remove Batch Effect function in "limma" package (13) in R was used to remove batch effect and combine the four datasets, and the removal of batch effect was evaluated by comparing the visual PCA (Principle Component Analysis) diagram before and after batch removal. There were a total of 79 tumor samples and 114 normal lung tissue samples in the combined GEO datasets. Additionally, the high throughput sequencing data of GSE40419 was acquired from the GEO database for immune-related analysis. There were 87 tumor samples and 77 adjacent normal lung tissue samples in the GSE40419 dataset.

Differential expression analysis of SLC2A1

The differential expression difference analysis and visualization of *SLC2A1* between tumor and normal tissues in pan-cancer and LUAD were analyzed using basic R package and "ggplot2" package (14) in R software. Subsequently, the TCGA samples were divided into a "high" and "low" group according to the expression of *SLC2A1*, and the cutoff value was the median expression value of *SLC2A1*. Baseline data tables describing the relationship between *SLC2A1* expression and various clinical information were drawn using the basic package in R. "Limma" package in R was used to study the differential expression of mRNAs (message RNAs) between the two groups. The adjusted P value was analyzed to correct for false positive results. "Adjusted P<0.05 and Log(Fold Change) >1 or Log(Fold Change) <–1" were defined as the thresholds for screening the differential expression of mRNAs. A Volcano plot and cluster heatmap were constructed using "gglot2" package in R to visualize the differential analysis results.

Prognosis-related analysis

The Gene Expression Profiling Interactive Analysis (GEPIA) (15) and Kaplan-Meier Plotter (16) website tools were applied to construct survival curve and evaluate the prognostic potential of *SLC2A1* in LUAD. The "median value" of *SLC2A1* expression was selected as the cutoff value in GEPIA for grouping, and the survival curves of all samples in both two groups were drawn with OS (overall survival) and PFS (progression free survival) as the end points, respectively. The same grouping was constructed using the Kaplan-Meier Plotter, and the survival curves of all samples and each clinical subgroup of the two groups were drawn with OS and PFS as the end points, respectively. In addition, univariate and multivariate Cox analyses were performed on *SLC2A1* and the clinical characteristics to assess the potential independent prognostic value of *SLC2A1* in LUAD using "glmnet" and "survival" packages (17,18) in R. The clinical characteristics of age, sex, smoking history and TNM stage were included in consideration of common clinical use and complete acquired data.

Gene Set Enrichment Analysis (GSEA) and Metascape annotation Analysis

GSEA was performed to further confirm the underlying function and obtain the relevant signaling pathways of *SLC2A1*-related differential expression genes in LUAD using "clusterProfiler" package (19) in R. The hallmark gene sets from GSEA-MSigDb (http://www.gsea-msigdb.org) were selected to conduct the GSEA. Gene Ontology (GO) and Kyoto Encyclopedia of Genes and Genomes (KEGG) enrichment analyses were also included. Metascape (https://metascape.org) (20) was used to perform the protein-protein interaction (PPI) enrichment analysis and disease-genetics analysis enrichment and tissue-specific enrichment analysis.

Tumor immune-related analysis

To investigate the role of *SLC2A1* in LUAD tumor immunity and its relationship with infiltrating immune cells, the "CIBERSORT" algorithm from the "immunedeconv" package (21) in R was used to calculate the immune-infiltrating score of TCGA samples. A heatmap was drawn to visualize the immune scores of the high and low *SLC2A1* expression groups, and the basic R package was then used to calculate whether there were significant differences in the immune-infiltration scores of 22 immune cells included in CIBERSORT between the two groups. Additionally, TIMER2.0 (http://timer.comp-genomics.org) (22) was used to calculate the immune-infiltrating score of GSE40419 tumor samples (n=87), and the "ggstatsplot" package (23) in R was applied to conduct the correlation analysis between *SLC2A1* and immune cells, in order to validate the "CIBERSORT" analysis results. *SIGLEC15*, *TIGIT*, *CD274*, *HAVCR2*, *PDCD1*, *CTLA4*, *LAG3*, and *PDCD1LG2* are immune checkpoint-related transcripts (24-27). The expression values of these eight genes were extracted to observe the expression of immune checkpoint-related genes in the high and low *SLC2A1* expression groups based on the TCGA samples. Also, the Tumor Immune Dysfunction and Exclusion (TIDE) algorithm (28) was used to predict the

response of the high and low *SLC2A1* expression groups to Immune-checkpoint-blocking (ICB) based on the TCGA samples.

Drug sensitivity analysis

The "pRRophetic" package (29) in R was used to assess the sensitivity of the high and low SLC2A1 expression groups to eight LUAD drugs included in the Cancer Genome Project (CGP) database (version cgp2016), including six chemotherapeutic drugs and two targeted drugs. The "ggplot2" package in R was applied to visualize the results, and TCGA samples were used to perform this analysis. In order to determine whether the relationship between SLC2A1 expression and sensitivity to targeted drugs is affected by differences in driver gene mutations, we used the "mafftools" package (30) in R to analyze the somatic mutations of patients. Using SPSS (version 26.0.0.0©, Copyright IBM Corporation 2021), we compared the high and low SLC2A1 expression groups to assess whether there were differences in the LUAD driver gene mutation frequency between both groups of patients.

Statistical analysis

The driver gene mutation frequency differences between the high and low *SLC2A1* expression groups were assessed using SPSS (version 26.0.0.0), and the other statistical analyses were performed in R software (version 4.1.0) (except for the online website tools mentioned above). The correlation analysis between *SLC2A1* expression and immune-infiltrating cells was assessed using the Pearson correlation coefficient. For all analyses, the low and high *SLC2A1* expression groups were established according to the median *SLC2A1* mRNA expression value in the selected dataset.

In the univariate and multivariate Cox regression analyses, *SLC2A1* was also divided into two grade variables "high" and "low" according to the median value. The paired t-test was used to compare the *SLC2A1* expression levels in TCGA tumor and pan-cancer paired samples. Pearson's chi-squared test was applied to analyze the differences in driver gene mutation frequency between the high and low *SLC2A1* expression groups (*P<0.05, **P<0.01, and ***P<0.001). All differences between groups (except those mentioned above) were analyzed using the unpaired t-test. P<0.05 (two-sided) was considered significant in all tests.

Results

SLC2A1 was highly expressed in LUAD tissues

By analyzing the expression of *SLC2A1* in the pan-cancer dataset included in TCGA database, we obtained the expression differences of *SLC2A1* in 33 cancers and the corresponding normal tissues (*Figure 1A*). The results showed that *SLC2A1* was significantly highly expressed in LUAD. The expression differential analysis results in the TCGA-LUAD dataset showed that the expression level of *SLC2A1* in LUAD tissues was higher than that in their adjacent tissues using both unpaired and paired sample *t*-tests (*Figure 1B,1C*).

The combined GEO data obtained was then used for the same analysis for a validation, and the results were consistent with those in TCGA data (*Figure 1D-1F*). This indicated that *SLC2A1* was more highly expressed in transcriptional levels in LUAD tissues than in normal lung tissues.

Overexpression of SLC2A1 indicated poor prognosis in LUAD

To explore the correlation between *SLC2A1* and the clinical phenotype of LUAD, we analyzed the expression of *SLC2A1* in each clinical subgroup of the TCGA-LUAD dataset (*Table 1*). The results showed that *SLC2A1* expression was significantly associated with T stage classification (P<0.001), N stage classification (P=0.015), TNM stage classification (P=0.002), gender (P=0.004), OS (P<0.001), and DSS (Disease Specific Survival) (P<0.001).

To further confirm the role of *SLC2A1* in the prognosis of LUAD, univariate and multivariate Cox regression analyses were performed. The results showed that high *SLC2A1* expression was associated with poorer prognosis in both univariate [HR (hazard ratio) (high *vs.* low) =1.689, 95% confidence interval (CI): 1.242–2.249, P<0.001] and multivariate [HR (high *vs.* low) =1.567, 95% CI: 1.127–2.179, P=0.008] regression in LUAD (*Figure 2A,2B*).

In order to more intuitively understand the relationship between *SLC2A1* and the survival of LUAD patients, GEPIA and the Kaplan-Meier Plotter were used to draw the survival curves of the high and low *SLC2A1* expression groups. GEPIA used TCGA-LUAD dataset, while the Kaplan-Meier Plotter used data from the site's own pre-processed GEO database. In the Kaplan-Meier Plotter, patients in the high and low SLC2A1 expression

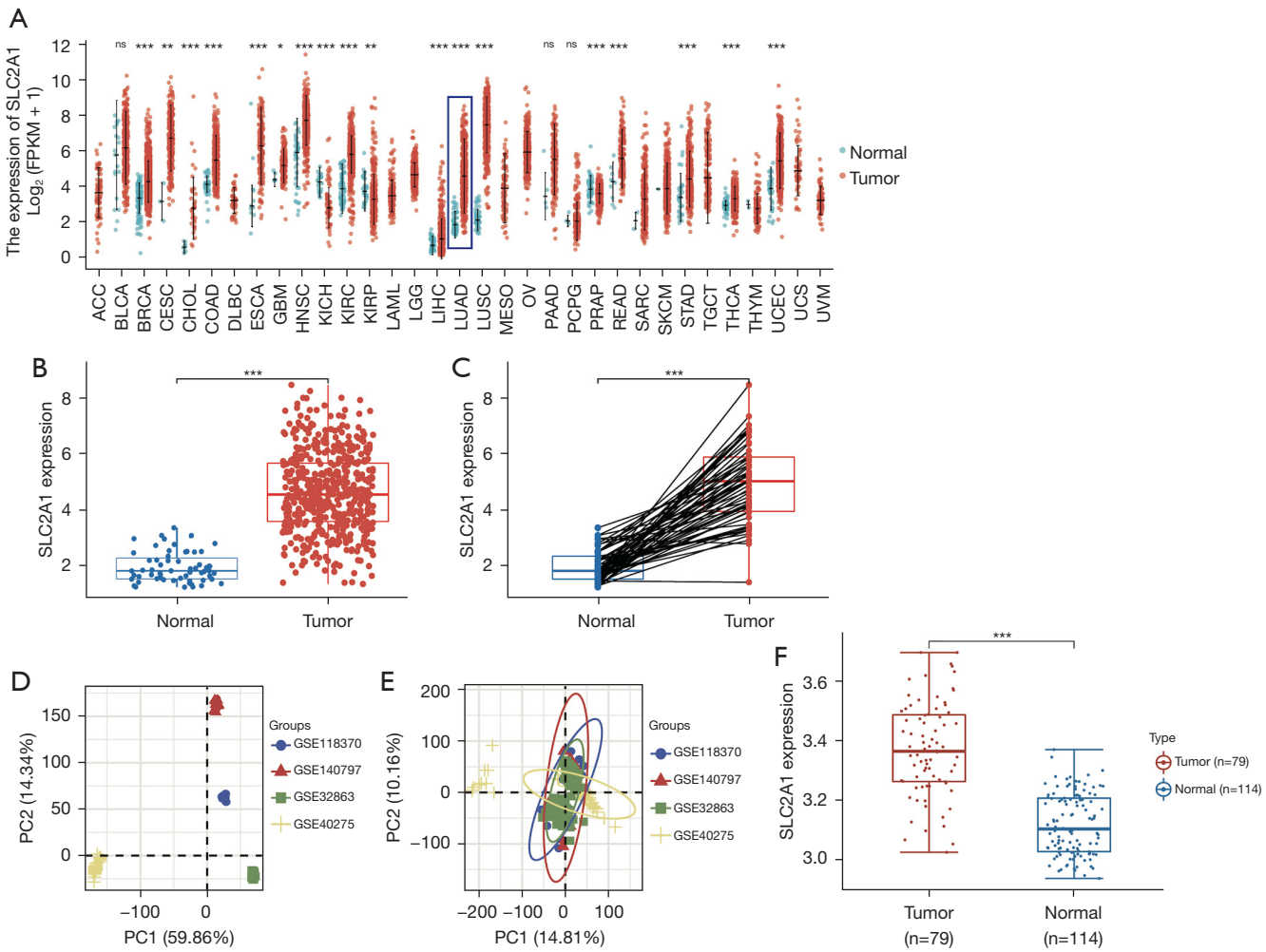

Figure 1 SLC2A1 was highly expressed in LUAD tissues. (A) The expression differences of SLC2A1 in 33 cancers and the corresponding normal tissues; (B) the expression level of SLC2A1 in LUAD tissues was higher than that in their adjacent tissues using unpaired sample *t*-test in TCGA data; (C) the expression level of SLC2A1 in LUAD tissues was higher than that in their adjacent tissues using paired sample *t*-test in TCGA data; (D) the PCA diagram of the four GEO datasets before batch removal; (E) the PCA diagram of the four GEO datasets after batch removal; (F) SLC2A1 was more highly expressed in transcriptional levels in LUAD tissues than in normal lung tissues in the GEO data. *, P<0.05; **, P<0.01; ***, P<0.001; ns, P>0.05. LUAD, lung adenocarcinoma; LUSC, lung squamous cell carcinoma; TCGA, The Cancer Genome Atlas; GEO, Gene Expression Omnibus; PCA, principal components analysis.

groups exhibited significant differences in OS and PFS (*Figure 2C*,*2D*). In addition, we also compared the OS and PFS of the two groups in various clinical subgroups, such as male, female, smoking, non-smoking, postoperative, and post-chemotherapy, and the results showed that high *SLC2A1* expression predicted poor prognosis in both the overall samples as well as the samples of each subgroup (*Figure 2C-2O*). GEPIA survival analysis showed that the high *SLC2A1* expression group had significantly worse OS than the low expression group (HR =1.9, logrank P=2.4e-05) (*Figure 2P*). However, through GEPIA, we found that the PFS of the two groups were not significantly different in the logrank test (logrank P=0.053) (*Figure 2Q*). Based on these results, we concluded that *SLC2A1* expression is significantly related to the progression and survival of LUAD.

Functional enrichment analysis and PPI network of SLC2A1-related differential genes

Analysis of the gene expression differences between the

Table 1 The expression of SLC2A1 in each clinical subgroup of the TCGA-LUAD dataset

Characteristic	Low SLC2A1 expression (n=267)	High SLC2A1 expression (n=268)	P value
T stage, n (%)			<0.001
T1	108 (20.3)	67 (12.6)	
T2	133 (25.0)	156 (29.3)	
T3	14 (2.6)	35 (6.6)	
T4	10 (1.9)	9 (1.7)	
N stage, n (%)			0.015
N0	186 (35.8)	162 (31.2)	
N1	38 (7.3)	57 (11.0)	
N2	30 (5.8)	44 (8.5)	
N3	0 (0)	2 (0.4)	
M stage, n (%)			0.225
M0	183 (47.4)	178 (46.1)	
M1	9 (2.3)	16 (4.1)	
Pathologic stage, n (%)			0.002
Stage I	168 (31.9)	126 (23.9)	
Stage II	51 (9.7)	72 (13.7)	
Stage III	33 (6.3)	51 (9.7)	
Stage IV	10 (1.9)	16 (3.0)	
Gender, n (%)			0.004
Female	160 (29.9)	126 (23.6)	
Male	107 (20.0)	142 (26.5)	
OS event, n (%)			<0.001
Alive	193 (36.1)	150 (28.0)	
Dead	74 (13.8)	118 (22.1)	
DSS event, n (%)			<0.001
Alive	208 (41.7)	171 (34.3)	
Dead	43 (8.6)	77 (15.4)	
PFS event, n (%)			0.007
Alive	170 (31.8)	139 (26.0)	
Dead	97 (18.1)	129 (24.1)	
Age, median [IQR]	67 [60, 73]	65 [58, 72]	0.135

T, tumor; N, node; M, metastasis; TCGA, The Cancer Genome Atlas; LUAD, lung adenocarcinoma; OS, overall survival; DSS, disease specific survival; PFS, progression free survival; IQR, interquartile range.

high and low *SLC2A1* expression groups in TCGA-LUAD showed that 306 genes exhibited significant expression differences [adj. P<0.05, abs (log2FC(Fold Change)) >1], among which 179 genes were highly expressed and 127 genes were lowly expressed in the high *SLC2A1* group (*Figure 3A*, Figure S1). The difference analysis results are reported in detail in Table S1. We drew the expression heatmap of these 306 genes from the GEO data, and the results showed that there were significant differences in the expression of these genes in the high and low *SLC2A1* expression groups, which verified the results of TCGA data analysis (*Figure 3B*). Furthermore, GSEA showed that these 306 *SLC2A1*-related genes were closely related to the basic cellular activities (*Figure 4A-4C*, *Table 2*, Tables S2-S4). In terms of cellular components (CC), we found that these *SLC2A1*-related differential genes were primarily enriched in the extracellular region, intracellular anatomical structure, organelles, and nucleus. As for biological processes (BP), these genes were enriched in the cellular component organization, or more specifically, the cell cycle (according to the KEGG pathway analysis results). With regards to molecular function (MF), *SLC2A1* was found to be closely correlated with protein binding.

GSEA based on the HALLMARK gene set in MSigDb showed that these *SLC2A1*-related genes were mainly enriched in the G2M CHECKPOINT, E2F TARGETS, MITOTIC SPINDLE, GLYCOLYSIS, and MTORC1 SIGNALING pathways. By searching the annotation of GSEA of these five pathways, we found that the first three pathways were all related to the occurrence or development of mitosis. Thus, we hypothesized that these genes might have a lot to do with tumor progression, and subsequent functional enrichment analyses using Metascape confirmed our hypothesis.

The PPI network analysis results showed that these *SLC2A1*-related genes were mainly enriched in the resolution of sister chromatid cohesion, mitotic anaphase, and metaphase (*Table 3*, *Figure 5A,5B*). Moreover, the disease-genetics analysis result showed these genes were most concentrated in recurrent tumor (*Figure 6A*). More importantly, the tissue-specific enrichment analysis results showed that the *SLC2A1*-related genes were mainly enriched in lung tissue and bronchial epithelial cells (*Figure 6B*).

Relationship between SLC2A1 and tumor-infiltrating immune cells (TIICs) and the role of SLC2A1 in tumor immunity

Immune infiltration analysis using CIBERSORT revealed

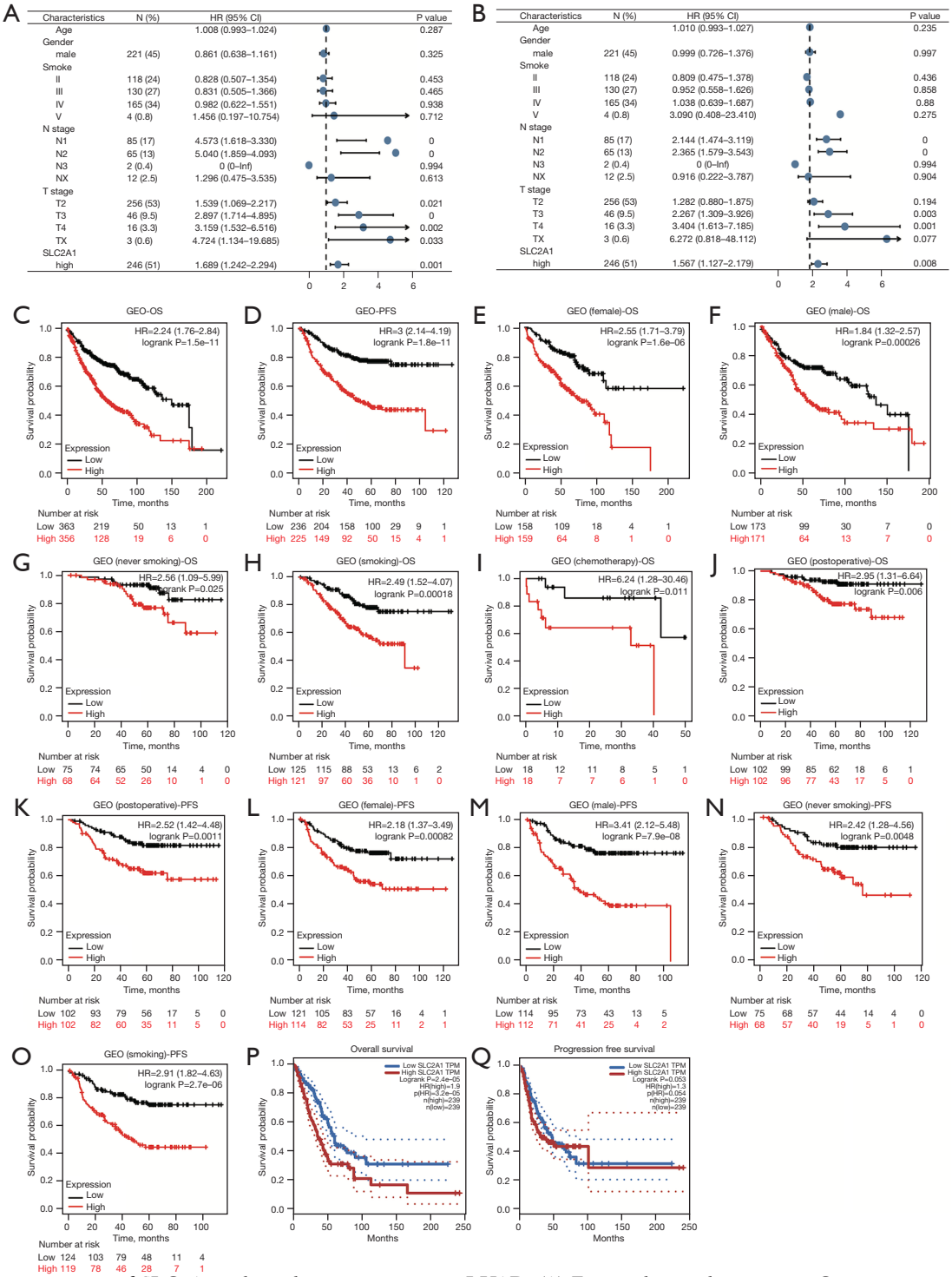

Figure 2 Overexpression of SLC2A1 indicated poor prognosis in LUAD. (A) Forest plots with univariate Cox regression for SLC2A1 and clinical factors; (B) Forest plots with multivariate Cox regression incorporating SLC2A1 and clinical factors; (C-O) high expression of SLC2A1 predicted poor OS and PFS in both the overall samples and each subgroup samples in the Kaplan-Meier Plotter; (P) the high SLC2A1 expression group had significantly worse OS than the low SLC2A1 expression group in GEPIA; (Q) the PFS of the two groups did not exhibit significant differences in the logrank test by GEPIA. LUAD, lung adenocarcinoma; OS, overall survival; PFS, progression free survival; GEPIA, Gene Expression Profiling Interactive Analysis.

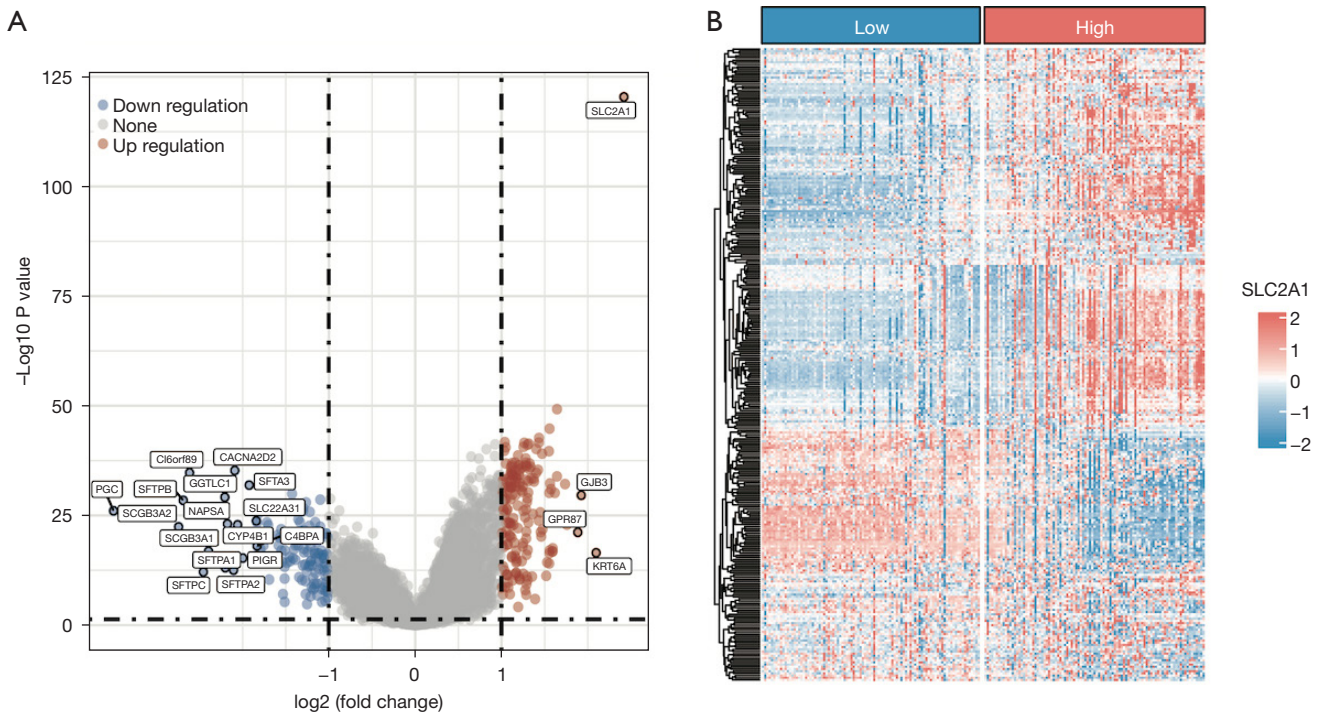

Figure 3 SLC2A1-related differential gene analysis in volcano map and heatmap. (A) Volcano map of SLC2A1-related differential gene analysis using TCGA data; (B) an expression heatmap of 306 differentially-expressed genes were drawn using the GEO data. TCGA, The Cancer Genome Atlas; GEO, Gene Expression Omnibus.

marked differences in the infiltration of nine types of immune cells between the high and low *SLC2A1* expression groups (*Figure 7A*). To verify this, we used GSE40419 to calculate the immune score in the TIMER database, and conducted correlation analysis between *SLC2A1* and 22 immune cells by CIBERSORT. The correlation analysis results showed that three of the nine immune cells that CIBERSORT considered to be different were correlated with *SLC2A1*, and the trend of two of these three cells was the same as TCGA results (*Figure 7B-7D*, Figure S2). According to the *Figure 7C,7D*, *SLC2A1* expression was positively correlated with activated $CD4^+$ memory T cells (r=0.31, P=0.003) and negatively correlated with activated mast cells (r=−0.28, P=0.010). The correlation between *SLC2A1* and these two types of cells in TCGA data was then evaluated using TIMER2.0, and the results were identical (*Figure 7E*).

Additionally, we also paid attention to the immune microenvironment score, immune score, and stromal score calculated by XCELL algorithm in TIMER, and found that *SLC2A1* expression was negatively correlated with the immune stromal score (r=−0.25, P=0.021) (*Figure 7F*). This indicated that *SLC2A1* plays an important role in tumor immune cells infiltrating and it has a certain influence on the tumor immune microenvironment.

In order to explore the role of *SLC2A1* in the clinical application of tumor immunity, we also compared the expression of eight immune-checkpoint-related transcripts between the high and low *SLC2A1* expression groups. Additionally, the TIDE scores of these two groups were also calculated to compare the potential immune-checkpoint-blocking (ICB) response. The results showed that four of the eight immune-checkpoint-related genes were differentially expressed in both groups (*Figure 8A*). All four genes were highly expressed in the high *SLC2A1* expression group. Similarly, the TIDE score of the high *SLC2A1* expression group was markedly higher than that of the low *SLC2A1* expression group (*Figure 8B*). This suggested that patients with high *SLC2A1* expression may have a poor prognosis due to their own poor immune response to the tumor, and the effect of immunotherapy in these patients may be worse than that of patients with low *SLC2A1* expression.

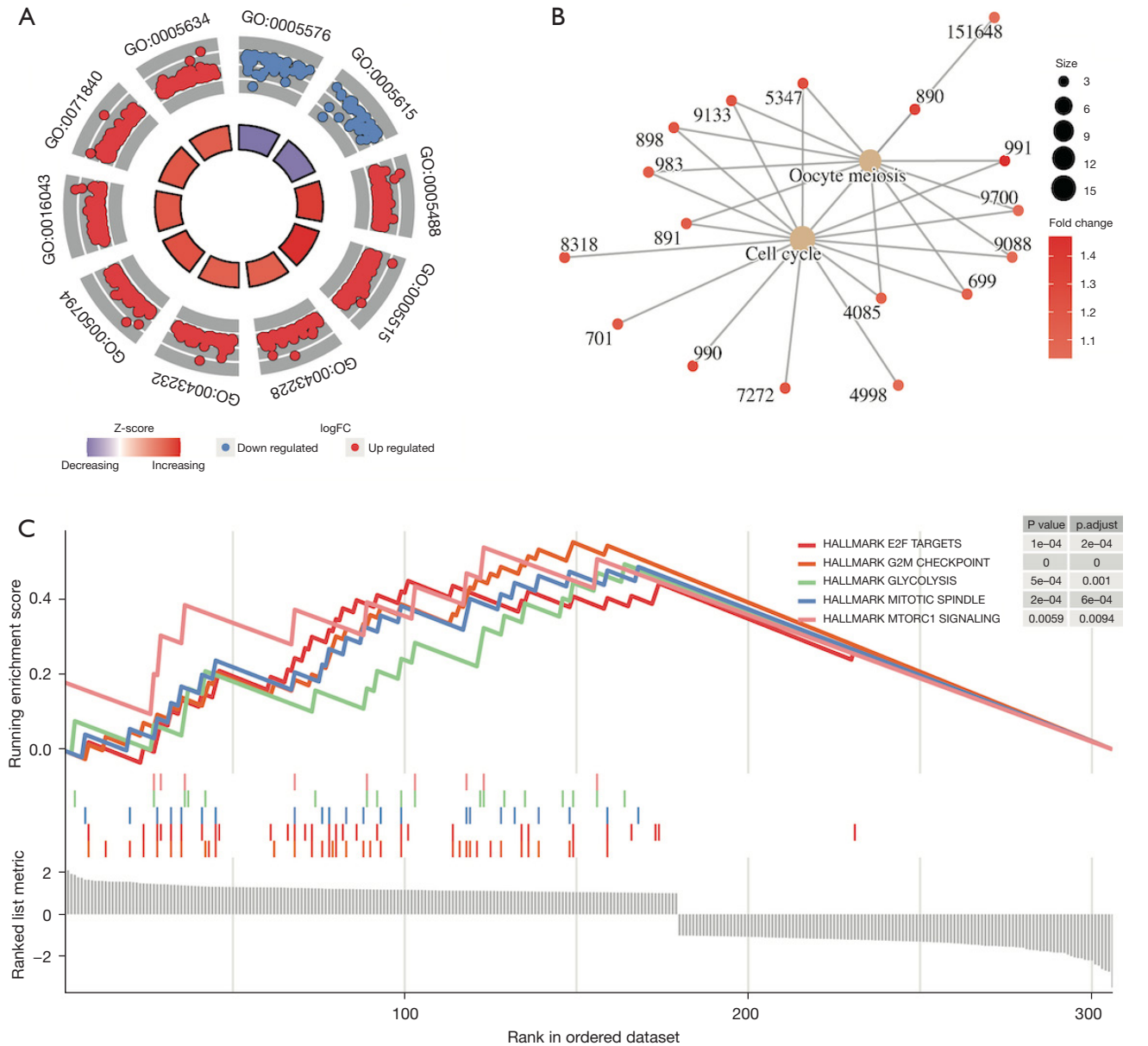

Figure 4 Functional enrichment analysis of SLC2A1-related differential genes by GSEA. (A) The results of GO analysis containing logFC for SLC2A1-related differential genes; (B) the results of KEGG analysis containing logFC for SLC2A1-related differential genes showed these SLC2A1-related genes were mainly enriched in the cell cycle; (C) Gene Set Enrichment Analysis based on the HALLMARK gene set in MSigDb showed that these SLC2A1-related genes were mainly enriched in the G2M CHECKPOINT, E2F TARGETS, MITOTIC SPINDLE, GLYCOLYSIS, and MTORC1 SIGNALING pathways. GSEA, Gene Set Enrichment Analysis; logFC, log (Fold Change); GO, Gene Ontology; KEGG, Kyoto Encyclopedia of Genes and Genomes; MSigDb, The Molecular Signatures Database.

Patients in the high and low SLC2A1 expression groups had different sensitivities to chemotherapy drugs and targeted drugs

We summarized the currently commonly used chemotherapy and targeted drugs for LUAD and matched them with drugs included in the CGP database, and found that eight therapeutic drugs were included in the CGP database. We used the gene expression profile data of the samples to

Table 2 Gene Set Enrichment Analysis results [including GO (top 10) and KEGG enrichment analysis] for SLC2A1-related differential genes

ID	Description	Enrichment score	P.adjust
GO:0005576	Extracellular region	–0.292583838	0.016661795
GO:0005615	Extracellular space	–0.338404417	0.016661795
GO:0005488	Binding	0.358355609	0.016661795
GO:0005622	Intracellular anatomical structure	0.249840001	0.016661795
GO:0043228	Non-membrane-bounded organelle	0.351254306	0.016661795
GO:0043232	Intracellular non-membrane-bounded organelle	0.351254306	0.016661795
GO:0050794	Regulation of cellular process	0.2390881	0.016661795
GO:0005515	Protein binding	0.341020358	0.016661795
GO:0005634	Nucleus	0.29956241	0.016661795
GO:0016043	Cellular component organization	0.349091002	0.016661795
hsa04110	Cell cycle	0.506896552	0.005719886
hsa04114	Oocyte meiosis	0.484745763	0.018079801
HALLMARK_G2M_CHECKPOINT	HALLMARK_G2M_CHECKPOINT	0.551469393	3.20E-07
HALLMARK_E2F_TARGETS	HALLMARK_E2F_TARGETS	0.448623465	2.87E-04
HALLMARK_MITOTIC_SPINDLE	HALLMARK_MITOTIC_SPINDLE	0.485915493	4.95E-04
HALLMARK_GLYCOLYSIS	HALLMARK_GLYCOLYSIS	0.493055556	0.001923517
HALLMARK_MTORC1_SIGNALING	HALLMARK_MTORC1_SIGNALING	0.537546645	0.015472396

GO, Gene Ontology; KEGG, Kyoto Encyclopedia of Genes and Genomes.

predict the IC50 of the two groups, and the results showed that the sensitivity of patients with low *SLC2A1* expression to six chemotherapy drugs was significantly higher than that of patients with high *SLC2A1* expression (*Figure 9A-9F*), while patients with high *SLC2A1* expression were markedly more sensitive to the two targeted therapies than those with low *SLC2A1* expression (*Figure 9G,9H*). We considered that this may be due to differences in the somatic mutations between patients with high and low *SLC2A1* expression, and the mutation frequency of driver genes in patients with high *SLC2A1* expression may be higher.

Therefore, we conducted a landscape analysis of mutations in *SLC2A1* high and low expression groups using R, and the results showed that there was no notable difference in the top 10 mutant genes between the two groups (Figures S3,S4). According to the mutation frequency difference analysis between the two groups (Figure S5), there were significant differences in *ALK*, *MET*, and *ROS1* mutations between the two groups. However, the mutation of *EGFR*, which was the target of the two targeted drugs for drug sensitivity analysis, showed no significant difference between the two groups. Therefore, we believe that this cannot explain the above drug sensitivity analysis results, and further research may be needed to determine the specific reasons.

Discussion

At present, it has been established that the growth and diffusion of a tumor depends on the characteristics of the tumor cells themselves, and is also closely related to the internal tumor microenvironment, especially the tumor immune microenvironment (31-33). Previous study (11) has shown that *SLC2A1* is overexpressed in LUAD tumor tissues and has prognostic significance for patients with surgically-resected LUAD. However, the prognostic role of *SLC2A1* transcription in all LUAD patients, its possible mechanism, and its role in tumor immunity have not yet been established.

In this study, *SLC2A1* was found to be significantly overexpressed in LUAD tumor tissues and associated with poor prognosis. Univariate and multivariate Cox regression

Table 3 PPI network analysis results for SLC2A1-related differential genes

MCODE	ID	Description	Log10(P)
MCODE_1	R-HSA-2500257	Resolution of Sister Chromatid Cohesion	–44
MCODE_1	R-HSA-68882	Mitotic Anaphase	–41.9
MCODE_1	R-HSA-2555396	Mitotic Metaphase and Anaphase	–41.9
MCODE_2	R-HSA-163125	Post-translational modification: synthesis of glycosylphosphatidylinositol (GPI)-anchored proteins	–11.3
MCODE_2	R-HSA-6798695	Neutrophil degranulation	–7
MCODE_2	GO:0031638	zymogen activation	–5.4
MCODE_3	R-HSA-983189	Kinesins	–6.8
MCODE_3	R-HSA-6811434	Coat protein complex I (COPI)-dependent Golgi-to-endoplasmic reticulum (ER) retrograde traffic	–6.1
MCODE_3	R-HSA-2132295	Major histocompatibility complex (MHC) class II antigen presentation	–5.8
MCODE_4	R-HSA-6809371	Formation of the cornified envelope	–11.7
MCODE_4	R-HSA-6805567	Keratinization	–10.6
MCODE_4	GO:0002009	morphogenesis of an epithelium	–4.2
MCODE_5	R-HSA-5688890	Defective CSF2RA causes SMDP4	–18.8
MCODE_5	R-HSA-5688849	Defective CSF2RB causes SMDP5	–18.8
MCODE_5	R-HSA-5687613	Diseases associated with surfactant metabolism	–18.1
MCODE_6	R-HSA-983189	Kinesins	–10.8
MCODE_6	R-HSA-6811434	COPI-dependent Golgi-to-ER retrograde traffic	–9.8
MCODE_6	R-HSA-8856688	Golgi-to-ER retrograde transport	–9.3
MCODE_7	R-HSA-1650814	Collagen biosynthesis and modifying enzymes	–10.5
MCODE_7	R-HSA-1474290	Collagen formation	–10
MCODE_7	R-HSA-1474244	Extracellular matrix organization	–7.9
MCODE_8	R-HSA-418594	G alpha (i) signaling events	–7.8
MCODE_8	R-HSA-373076	Class A/1 (Rhodopsin-like receptors)	–7.7
MCODE_8	R-HSA-500792	g-protein coupled receptor (GPCR) ligand binding	–7.1
MCODE_9	GO:0000079	regulation of cyclin-dependent protein serine/threonine kinase activity	–7.4
MCODE_9	GO:1904029	regulation of cyclin-dependent protein kinase activity	–7.3
MCODE_9	WP179	Cell cycle	–7.1
MCODE_10	R-HSA-8957275	Post-translational protein phosphorylation	–7.3
MCODE_10	R-HSA-381426	Regulation of insulin-like growth factor (IGF) transport and uptake by insulin-like growth factor binding proteins (IGFBPs)	–7.1
MCODE_11	M65	PID FRA PATHWAY	–8.7
MCODE_11	M167	PID AP1 PATHWAY	–7.8

PPI, protein-protein interaction.

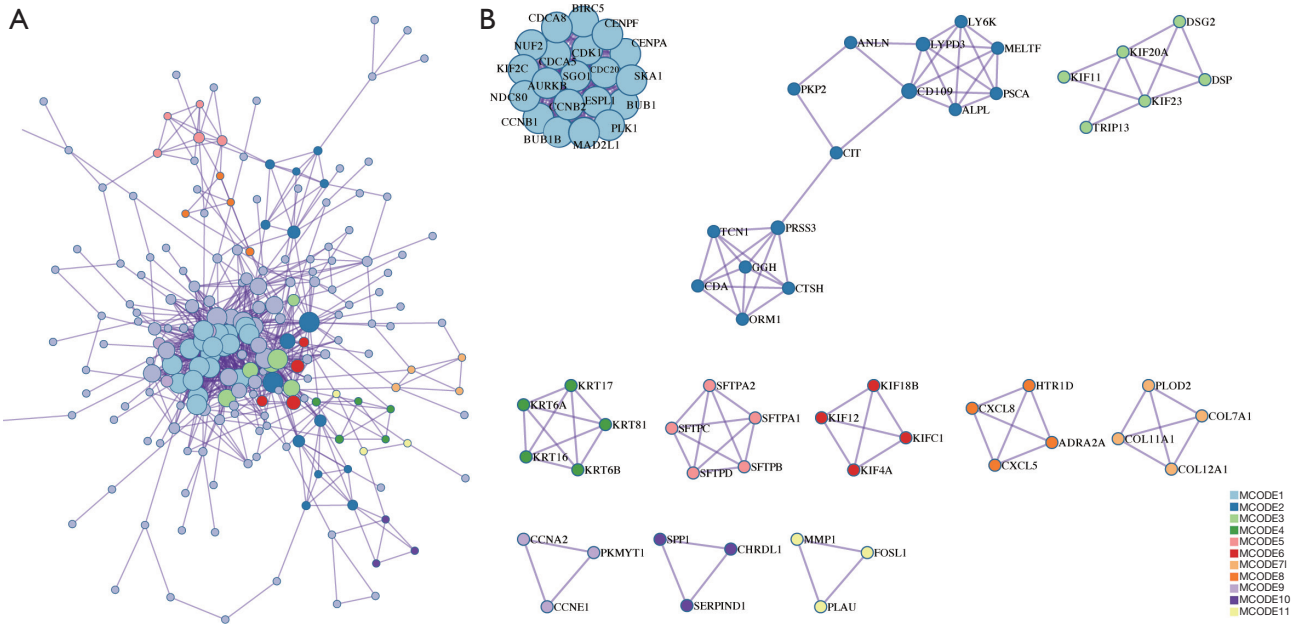

Figure 5 PPI network of SLC2A1-related differential genes. (A) PPI network of SLC2A1-related differential genes; (B) the 11 key nodes that make up this PPI network and the genes contained within. PPI, protein-protein interaction.

analyses showed that *SLC2A1* is an independent prognostic biomarker of LUAD. Next, we constructed the differential expression and PPI networks of *SLC2A1*, and the potential mechanism of *SLC2A1* in LUAD was explored. We subsequently explored the relationship between *SLC2A1* and tumor immunity, and found that *SLC2A1* is correlated with tumor immune invasion and immunotherapy efficacy, which may be a possible reason for the correlation between *SLC2A1* and poor prognosis. Finally, the relationship between *SLC2A1* and drug sensitivity was analyzed. Our study systematically revealed the role of *SLC2A1* as a tumor prognostic marker in LUAD, and analyzed its potential mechanism and clinical significance from various aspects.

Through further analysis of TCGA-LUAD data, we found that *SLC2A1* expression varied among T stages, N stages, and different genders. We then performed survival analysis using GEPIA and the Kaplan-Meier Plotter, and found that high *SLC2A1* expression was associated with worse OS and PFS. Our results suggest that *SLC2A1* has potential as a diagnostic and prognostic biomarker for LUAD. However, the biological function of *SLC2A1* and its potential prognosis-related mechanism still needs to be explored.

In order to explore the potential molecular mechanism of *SLC2A1* in LUAD, *SLC2A1*-related differential expression analysis was performed on TCGA-LUAD data and a *SLC2A1* differential expression network was constructed. In total, 306 *SLC2A1*-related differential expression genes were screened out. GO and KEGG analyses of these genes revealed that they were mainly concentrated in cell cycle and mitosis-related pathways. The GSEA enrichment analysis results with the HALLMARK gene sets as the background showed that these genes were mainly enriched in the G2M CHECKPOINT, E2F TARGETS, MITOTIC SPINDLE, GLYCOLYSIS, and MTORC1 SIGNALING pathways. G2/M checkpoint has been reported to play a role in DNA repair in tumor cells (34). Normal cells repair DNA damage during G1 arrest, which is often deficient in cancer cells, while cancer cells repair damaged DNA depending on the G2/M checkpoint. It has been reported that the G2/M checkpoint is associated with the development of multiple tumors (35). E2F TARGETS gene sets containing genes encoding cell cycle-related targets of E2F transcription factors, which are key regulators of cell cycle checkpoints, and regulate a large number of genes related to DNA replication and cell cycle progression (36). Furthermore, it has also been found to be associated with tumor progression (37,38). Similarly, MITOTIC SPINDLE, GLYCOLYSIS (39,40), and MTORC1 SIGNALING (41,42) have all been shown to play different

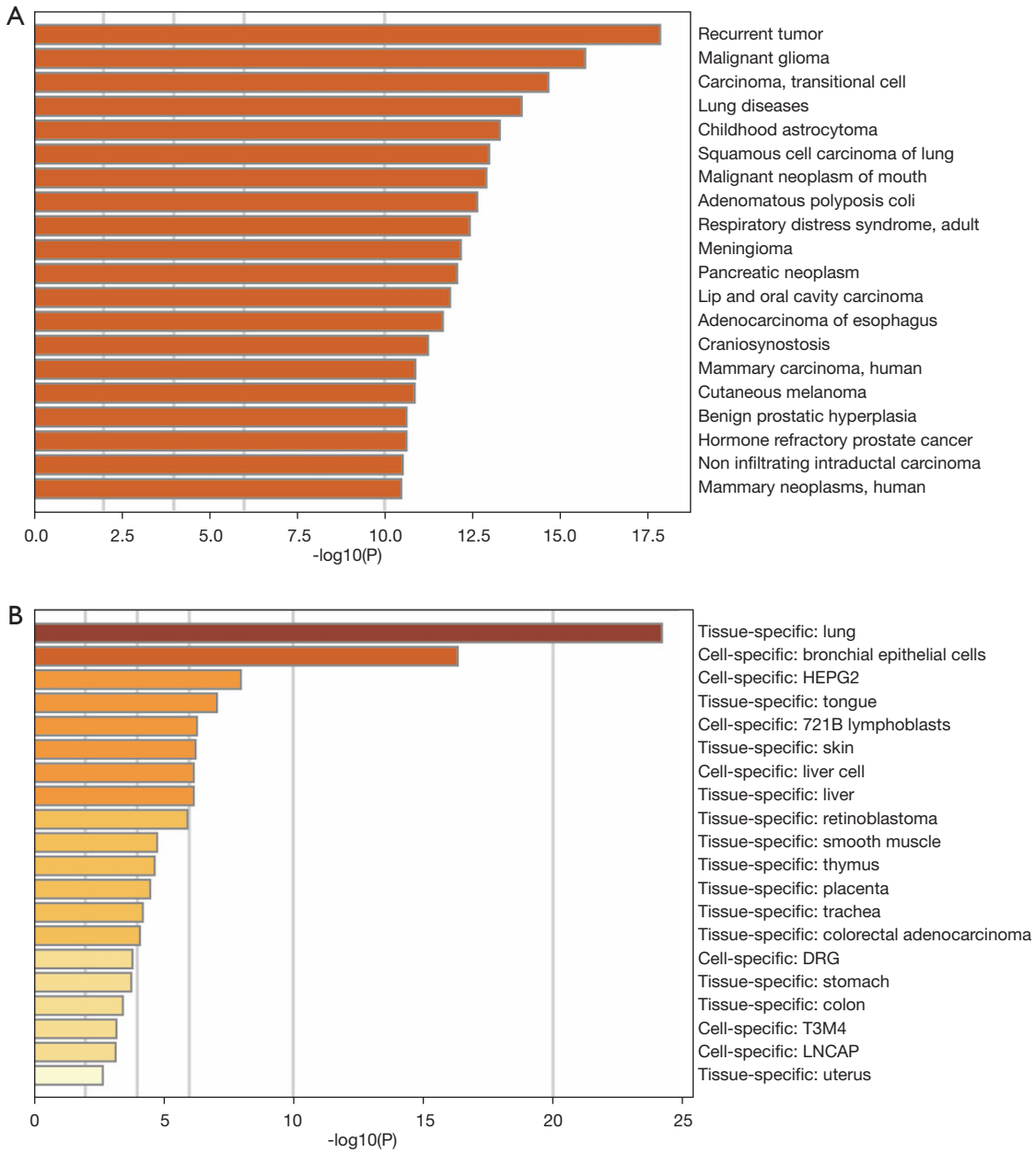

Figure 6 Disease-genetics analysis of SLC2A1-related differential genes. (A) The disease-genetics analysis result showed these genes were most concentrated in recurrent tumors; (B) the tissue-specific enrichment analysis results showed that the SLC2A1-related genes were mainly enriched in lung tissue and bronchial epithelial cells.

regulatory roles in tumor cell growth and the cell cycle. The Metascape enrichment analysis results provided more insight into protein, tissue, and disease levels. PPI showed that *SLC2A1*-related differential genes were mainly manifested in the resolution of sister chromatid cohesion, mitotic anaphase, and metaphase in terms of protein function, which were all associated with cell growth. In the tissue specific enrichment analysis, these genes were mainly expressed in lung tissue, bronchial epithelial cells, and the trachea. More importantly, the disease-genetics enrichment analysis results showed that the most closely related diseases were tumor recurrence and lung disease.

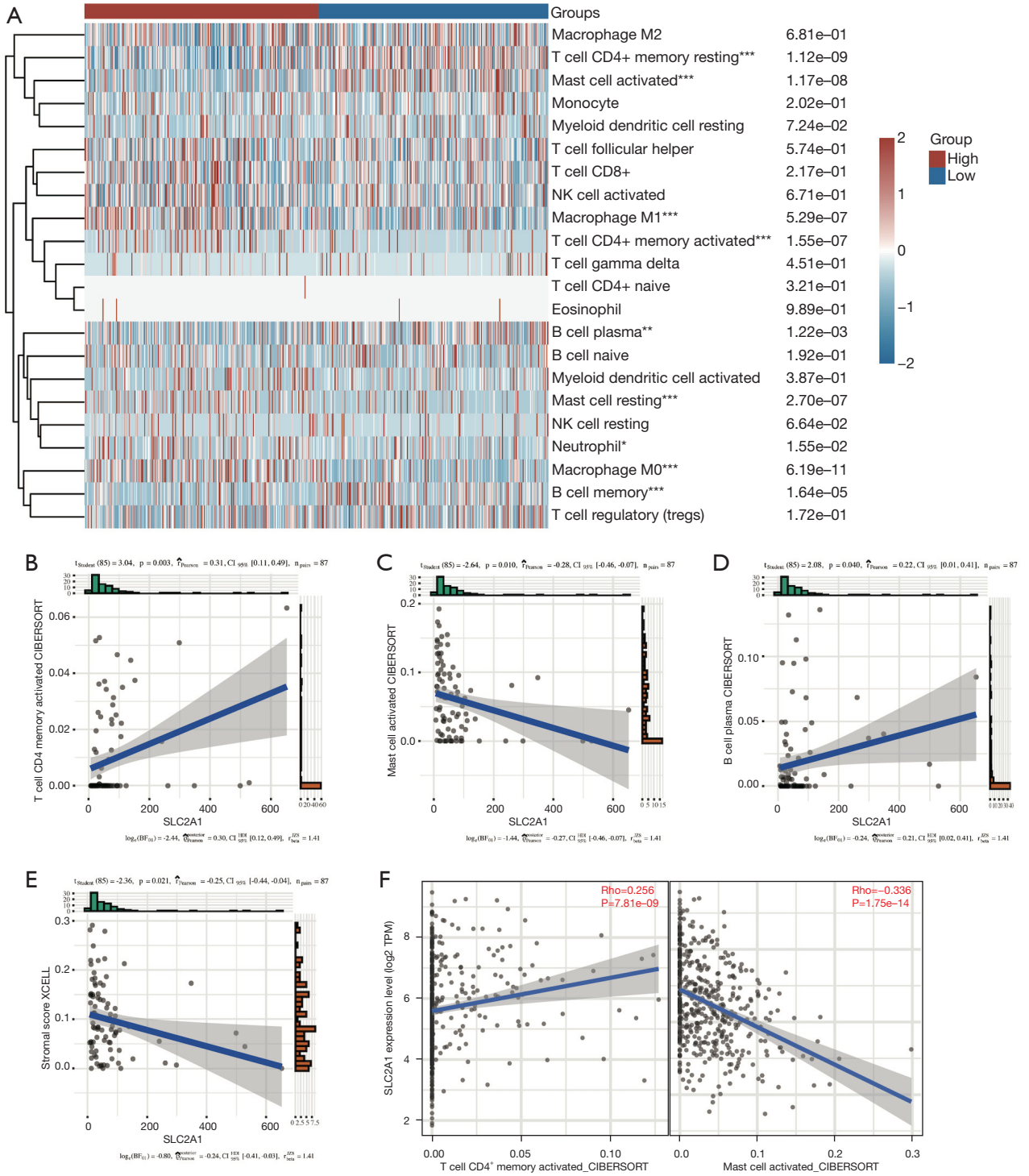

Figure 7 Relationship between SLC2A1 and tumor-infiltrating immune cells. (A) Immune infiltration analysis using CIBERSORT revealed significant differences in the infiltration of nine types of immune cells between the high and low SLC2A1 expression groups in TCGA; (B-D) three of the above nine tumor-infiltrating immune cells also exhibited a significant correlation with SLC2A1 in the GEO data, but the correlation trend of plasma B cells was contrary to that of the previous analysis; (E) SLC2A1 expression was negatively correlated with the stromal score in TIMER; (F) the correlation between SLC2A1 and the two cells in TCGA data was evaluated using TIMER2.0, and the results were the identical to those of the GEO. *, P<0.05; **, P<0.01; ***, P<0.001. TCGA, The Cancer Genome Atlas; GEO, Gene Expression Omnibus.

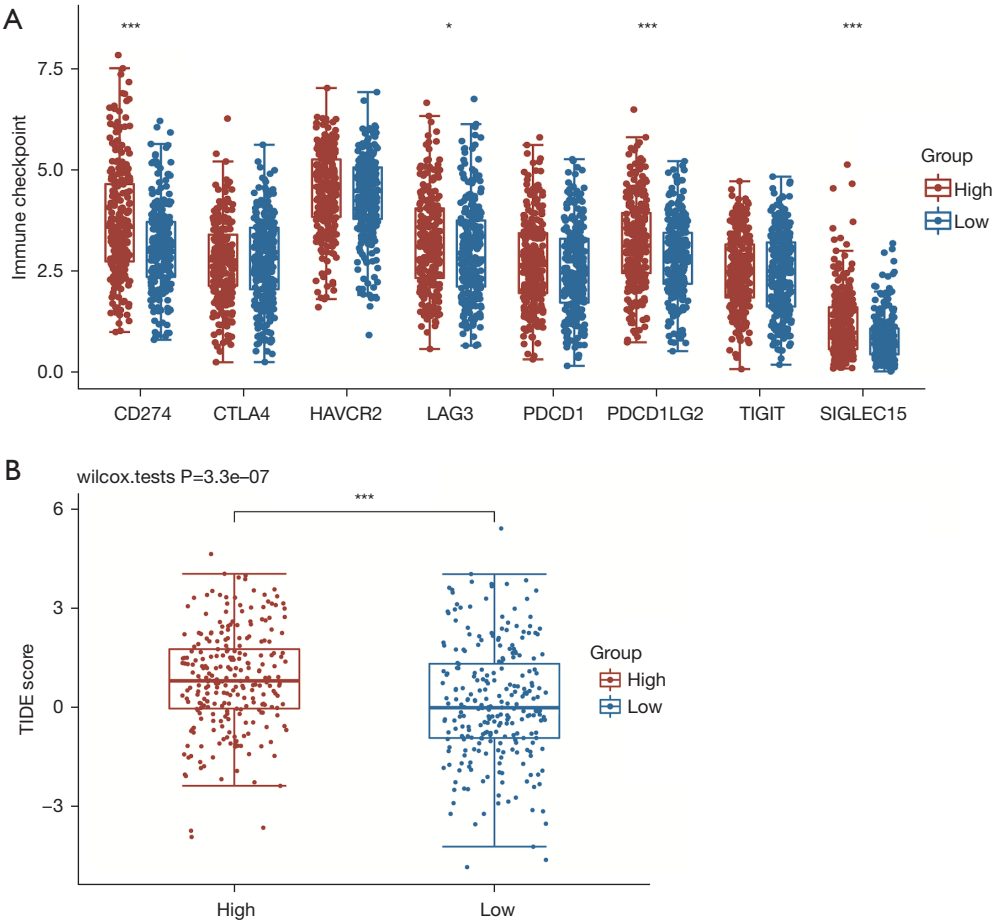

Figure 8 SLC2A1 was correlated with immune-checkpoint-transcripts and immune-checkpoint-blocking. (A) Four of the eight immune-checkpoint-related genes were differentially expressed in the two groups, and all four genes were highly expressed in the high SLC2A1 expression group; (B) the TIDE score of the high SLC2A1 expression group was significantly higher than that of the low SLC2A1 expression group. *, P<0.05; ***, P<0.001. TIDE, tumor immune dysfunction and exclusion.

These results directly illustrate the role of *SLC2A1* in lung tumor development and perfectly explain its prognostic role in LUAD.

However, according to the analysis results, *SLC2A1* may also play an important role in lung squamous cell carcinoma (LUSC). As shown in *Figure 1A*, the expression of *SLC2A1* in lung squamous cell carcinoma tissues is significantly higher than that in normal tissues. However, we plotted the survival curves of LUSC patients with high and low *SLC2A1* expression in GEPIA (Figure S6), and found no difference in survival between the two groups (logrank P_{OS} =0.22, P_{PFS} =0.3). This suggests that *SLC2A1* may be a good diagnostic indicator in LUSC, but is not associated with LUSC prognosis.

It is known that tumor immune infiltration is significantly associated with cancer prognosis (43). Therefore, we attempted to explore the relationship between *SLC2A1* and LUAD in terms of tumor immunity. We found that there were significant differences in the infiltration of nine infiltrating immune cells in the high and low *SLC2A1* expression groups, based on TCGA-LUAD data. After validation in the GEO data, we found that *SLC2A1* was positively correlated with activated $CD4^+$ memory T cells and negatively correlated with activated mast cells. Different immune infiltrations can lead to different outcomes in tumors (43,44). For example, activated $CD4^+$ memory T cell infiltration has been shown to be associated with poor prognosis and immune therapy response in several cancers (45,46), as have activated mast cells (47-49). This indicates that *SLC2A1* might play a vital role in regulating the tumor

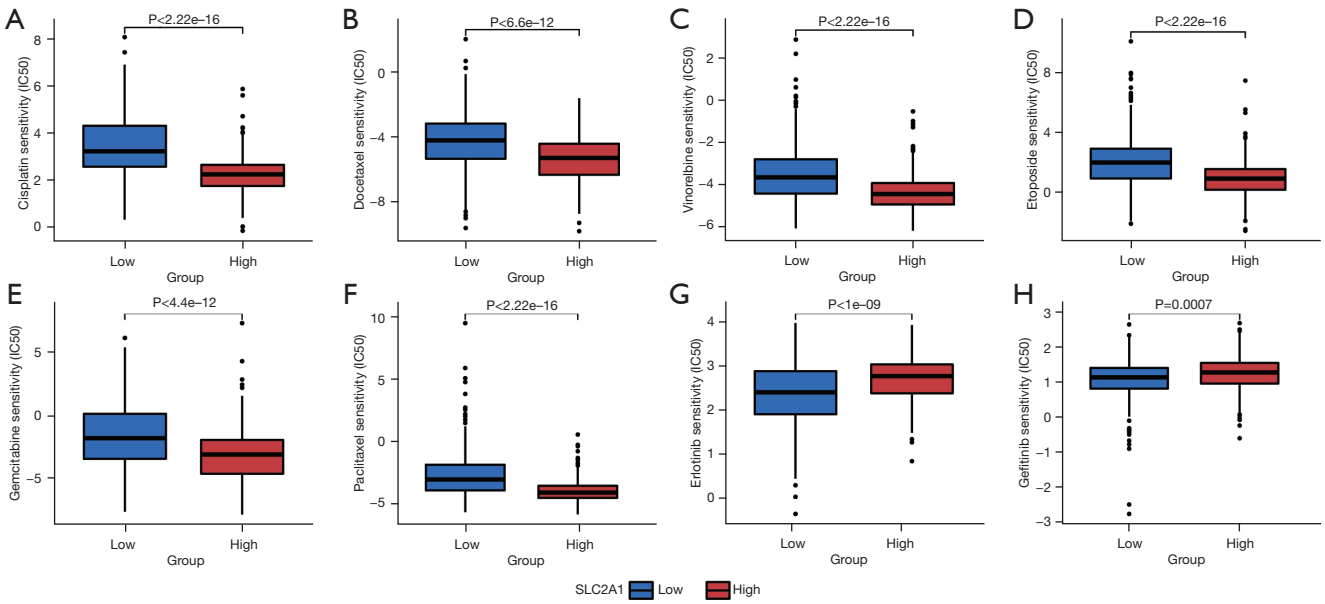

Figure 9 Patients with high and low SLC2A1 expression had different sensitivities to chemotherapy drugs and targeted drugs. (A-F) The sensitivity of patients with low SLC2A1 expression to six chemotherapy drugs was significantly higher than that of patients with high SLC2A1 expression; (G,H) patients with high SLC2A1 expression were significantly more sensitive to the two targeted therapies than those with low SLC2A1 expression.

immune microenvironment, and affects the prognosis of tumors by regulating infiltrating immune cells.

However, it is not just immune cell infiltration that affects the body's immune response to tumors. Immune checkpoint molecules are inhibitory regulatory molecules in the immune system, which are essential for maintaining tolerance, preventing autoimmune reactions, and minimizing tissue damage by controlling the timing and intensity of immune responses (50,51). The expression of immune checkpoint molecules will inhibit the function of immune cells, so that the body cannot produce an effective anti-tumor immune response, and the tumor will form immune escape (52,53). We screened out eight genes (24-27) associated with immune checkpoint via a literature search, and found that the expressions of four genes in the *SLC2A1* high expression group were significantly higher compared to the *SLC2A1* low expression group. This indicates that in the *SLC2A1* overexpression group, the function of immune cells is relatively suppressed and the risk of tumor immune escape is higher, which predicts a worse prognosis.

In addition, we also used the TIDE algorithm to evaluate the relationship between *SLC2A1* and the efficacy of immune checkpoint inhibitors. TIDE uses a set of gene expression markers to evaluate two different tumor immune escape mechanisms, including tumor-infiltrating cytotoxic T lymphocyte (CTL) dysfunction and rejection of CTL by immunosuppressive factors. A high TIDE score is associated with poor efficacy of immunocheckpoint blocking therapy (ICB) and short survival after ICB treatment. The TIDE score of the *SLC2A1* high expression group was significantly higher than that of the *SLC2A1* low expression group, indicating that patients with high *SLC2A1* had a relatively poor response to immune checkpoint inhibitors and a worse immunotherapy effect. These analyses strongly demonstrated that *SLC2A1* is closely associated to tumor immune cell infiltration and immune checkpoint, and provided an explanation as to why patients with high *SLC2A1* expression had worse prognosis in terms of tumor immunity.

Finally, we analyzed the relationship between *SLC2A1* and IC50(the half maximal inhibitory concentration) for LUAD therapy from a clinical perspective. The "pRRophetic" package is an algorithm for drug response prediction based on expression matrices developed by the CGP database, which contains 138 drug actions from more than 700 cell lines (29,54). Interestingly, we found that patients with high *SLC2A1* expression had remarkably

lower sensitivity to chemotherapy drugs than patients with low *SLC2A1* expression. This was consistent with the results of previous survival analyses of patients after chemotherapy. The Kaplan-Meier Plotter analysis showed that patients with high *SLC2A1* expression group had worse OS after chemotherapy, which may be largely attributable to a low sensitivity to chemotherapy drugs. Additionally, patients with high *SLC2A1* expression were more sensitive to targeted drugs, which we believe may be due to differences in somatic mutations between patients with high and low *SLC2A1* expression, and the driver gene mutation frequency of patients with high *SLC2A1* expression may be higher. However, subsequent mutation-related analyses refuted our hypothesis, and thus, further studies may be needed to investigate the cause of this susceptibility.

In order to avoid selection bias and increase the credibility of our research results, data from TCGA and GEO were used, and four different GEO datasets were utilized for joint analysis. However, our bioinformatics-based analysis still had limitations, and it is necessary for all research results to be verified by wet experiments. Also, the signaling pathway analyzed in this study was discovered through data mining, and its causal relationship in lung cancer needs to be verified experimentally. Finally, the number of tumor samples in the GEO dataset, which was used for validation, was relatively small. In future studies, we will expand the sample size and verify our analysis results in cell and animal models.

Conclusions

To the best of our knowledge, this is the first relatively complete study to reveal the role of *SLC2A1* in LUAD prognosis and tumor immunity, and determine the related mechanisms. Our study found that high *SLC2A1* expression in LUAD predicted poor prognosis and was closely related to tumor immunity, which could be used as an effective prognostic biomarker to provide a new strategy for clinical prognosis assessment and immunotherapy of LUAD.

Acknowledgments

Funding: This study was supported by the Project of Tianjin Key Clinical Disciplines and the Project of Tianjin Health Commission (grant No. ZD20023), and the Project of Tianjin Science and Technology Innovation Bureau (grant No. 20JCYBJC01350).

Footnote

Reporting Checklist: The authors have completed the REMARK reporting checklist. Available at https://atm.amegroups.com/article/view/10.21037/atm-22-1430/rc

Conflicts of Interest: All authors have completed the ICMJE uniform disclosure form (available at https://atm.amegroups.com/article/view/10.21037/atm-22-1430/coif). The authors have no conflicts of interest to declare.

Ethical Statement: The authors are accountable for all aspects of the work in ensuring that questions related to the accuracy or integrity of any part of the work are appropriately investigated and resolved. The study was conducted in accordance with the Declaration of Helsinki (as revised in 2013).

References

1. Siegel RL, Miller KD, Fuchs HE, et al. Cancer Statistics, 2021. CA Cancer J Clin 2021;71:7-33.
2. Barta JA, Powell CA, Wisnivesky JP. Global Epidemiology of Lung Cancer. Ann Glob Health 2019;85:8.
3. Devarakonda S, Masood A, Govindan R. Next-Generation Sequencing of Lung Cancers: Lessons Learned and Future Directions. Hematol Oncol Clin North Am 2017;31:1-12.
4. Kim IA, Hur JY, Kim HJ, et al. Targeted Next-Generation Sequencing Analysis for Recurrence in Early-Stage Lung Adenocarcinoma. Ann Surg Oncol 2021;28:3983-93.
5. Zhao X, Li X, Zhou L, et al. LncRNA HOXA11-AS drives cisplatin resistance of human LUAD cells via modulating miR-454-3p/Stat3. Cancer Sci 2018;109:3068-79.
6. Jin R, Wang X, Zang R, et al. Desmoglein-2 modulates tumor progression and osimertinib drug resistance through the EGFR/Src/PAK1 pathway in lung adenocarcinoma. Cancer Lett 2020;483:46-58.
7. Lin L, Yee SW, Kim RB, et al. SLC transporters as

therapeutic targets: emerging opportunities. Nat Rev Drug Discov 2015;14:543-60.
8. Mo Z, Yu L, Cao Z, et al. Identification of a Hypoxia-Associated Signature for Lung Adenocarcinoma. Front Genet 2020;11:647.
9. Wang X, Shi D, Zhao D, et al. Aberrant Methylation and Differential Expression of SLC2A1, TNS4, GAPDH, ATP8A2, and CASZ1 Are Associated with the Prognosis of Lung Adenocarcinoma. Biomed Res Int 2020;2020:1807089.
10. Su C, Liu WX, Wu LS, et al. Screening of Hub Gene Targets for Lung Cancer via Microarray Data. Comb Chem High Throughput Screen 2021;24:269-85.
11. Guo W, Sun S, Guo L, et al. Elevated SLC2A1 Expression Correlates with Poor Prognosis in Patients with Surgically Resected Lung Adenocarcinoma: A Study Based on Immunohistochemical Analysis and Bioinformatics. DNA Cell Biol 2020;39:631-44.
12. Ben Bolstad (2021). preprocessCore: A collection of pre-processing.functions. Available online: https://github.com/bmbolstad/preprocessCore
13. Ritchie ME, Phipson B, Wu D, et al. limma powers differential expression analyses for RNA-sequencing and microarray studies. Nucleic Acids Res 2015;43:e47.
14. Wickham H.. ggplot2: Elegant Graphics for Data Analysis. New York: Springer-Verlag, 2016.
15. Tang Z, Li C, Kang B, et al. GEPIA: a web server for cancer and normal gene expression profiling and interactive analyses. Nucleic Acids Res 2017;45:W98-W102.
16. Győrffy B, Surowiak P, Budczies J, et al. Online survival analysis software to assess the prognostic value of biomarkers using transcriptomic data in non-small-cell lung cancer. PLoS One 2013;8:e82241. Erratum in: PLoS One 2014;9:e111842.
17. Simon N, Friedman J, Hastie T, et al. Regularization Paths for Cox's Proportional Hazards Model via Coordinate Descent. J Stat Softw 2011;39:1-13.
18. Therneau T (2021). A Package for Survival Analysis in R_. R package version 3.2-11. Available online: https://CRAN.R-project.org/package=survival
19. Wu T, Hu E, Xu S, et al. clusterProfiler 4.0: A universal enrichment tool for interpreting omics data. Innovation (N Y) 2021;2:100141.
20. Zhou Y, Zhou B, Pache L, et al. Metascape provides a biologist-oriented resource for the analysis of systems-level datasets. Nat Commun 2019;10:1523.
21. Sturm G, Finotello F, List M. Immunedeconv: An R Package for Unified Access to Computational Methods for Estimating Immune Cell Fractions from Bulk RNA-Sequencing Data. Methods Mol Biol 2020;2120:223-32.
22. Li T, Fu J, Zeng Z, et al. TIMER2.0 for analysis of tumor-infiltrating immune cells. Nucleic Acids Res 2020;48:W509-14.
23. Patil I. Visualizations with statistical details: The 'ggstatsplot' approach. Journal of Open Source Software 2021;6:3167.
24. Zeng D, Li M, Zhou R, et al. Tumor Microenvironment Characterization in Gastric Cancer Identifies Prognostic and Immunotherapeutically Relevant Gene Signatures. Cancer Immunol Res 2019;7:737-50.
25. Ravi R, Noonan KA, Pham V, et al. Bifunctional immune checkpoint-targeted antibody-ligand traps that simultaneously disable TGFβ enhance the efficacy of cancer immunotherapy. Nat Commun 2018;9:741.
26. Wang J, Sun J, Liu LN, et al. Siglec-15 as an immune suppressor and potential target for normalization cancer immunotherapy. Nat Med 2019;25:656-66.
27. Yi L, Wu G, Guo L, et al. Comprehensive Analysis of the PD-L1 and Immune Infiltrates of m6A RNA Methylation Regulators in Head and Neck Squamous Cell Carcinoma. Mol Ther Nucleic Acids 2020;21:299-314.
28. Jiang P, Gu S, Pan D, et al. Signatures of T cell dysfunction and exclusion predict cancer immunotherapy response. Nat Med 2018;24:1550-8.
29. Geeleher P, Cox N, Huang RS. pRRophetic: an R package for prediction of clinical chemotherapeutic response from tumor gene expression levels. PLoS One 2014;9:e107468.
30. Mayakonda A, Lin DC, Assenov Y, et al. Maftools: efficient and comprehensive analysis of somatic variants in cancer. Genome Res 2018;28:1747-56.
31. Hanahan D, Weinberg RA. Hallmarks of cancer: the next generation. Cell 2011;144:646-74.
32. Matsushita H, Vesely MD, Koboldt DC, et al. Cancer exome analysis reveals a T-cell-dependent mechanism of cancer immunoediting. Nature 2012;482:400-4.
33. Steven A, Fisher SA, Robinson BW. Immunotherapy for lung cancer. Respirology 2016;21:821-33.
34. Matheson CJ, Backos DS, Reigan P. Targeting WEE1 Kinase in Cancer. Trends Pharmacol Sci 2016;37:872-81.
35. Vera J, Raatz Y, Wolkenhauer O, et al. Chk1 and Wee1 control genotoxic-stress induced G2-M arrest in melanoma cells. Cell Signal 2015;27:951-60.
36. Lavia P, Jansen-Dürr P. E2F target genes and cell-cycle checkpoint control. Bioessays 1999;21:221-30.
37. Bracken AP, Ciro M, Cocito A, et al. E2F target genes: unraveling the biology. Trends Biochem Sci

2004;29:409-17.
38. Tian W, Yang X, Yang H, et al. GINS2 Functions as a Key Gene in Lung Adenocarcinoma by WGCNA Co-Expression Network Analysis. Onco Targets Ther 2020;13:6735-46.
39. Feng J, Li J, Wu L, et al. Emerging roles and the regulation of aerobic glycolysis in hepatocellular carcinoma. J Exp Clin Cancer Res 2020;39:126.
40. Ganapathy-Kanniappan S, Geschwind JF. Tumor glycolysis as a target for cancer therapy: progress and prospects. Mol Cancer 2013;12:152.
41. Ben-Sahra I, Manning BD. mTORC1 signaling and the metabolic control of cell growth. Curr Opin Cell Biol 2017;45:72-82.
42. Takahara T, Amemiya Y, Sugiyama R, et al. Amino acid-dependent control of mTORC1 signaling: a variety of regulatory modes. J Biomed Sci 2020;27:87.
43. Pan Y, Sha Y, Wang H, et al. Comprehensive analysis of the association between tumor-infiltrating immune cells and the prognosis of lung adenocarcinoma. J Cancer Res Ther 2020;16:320-6.
44. Iglesia MD, Parker JS, Hoadley KA, et al. Genomic analysis of immune cell infiltrates across 11 tumor types. J Natl Cancer Inst 2016;108:djw144.
45. Gadi D, Griffith A, Tyekucheva S, et al. A T cell inflammatory phenotype is associated with autoimmune toxicity of the PI3K inhibitor duvelisib in chronic lymphocytic leukemia. Leukemia 2022;36:723-32.
46. Zou W, Li L, Wang Z, et al. Up-regulation of S100P predicts the poor long-term survival and construction of prognostic signature for survival and immunotherapy in patients with pancreatic cancer. Bioengineered 2021;12:9006-20.
47. Qiu P, Guo Q, Yao Q, et al. Characterization of Exosome-Related Gene Risk Model to Evaluate the Tumor Immune Microenvironment and Predict Prognosis in Triple-Negative Breast Cancer. Front Immunol 2021;12:736030.
48. Fan L, Ru J, Liu T, et al. Identification of a Novel Prognostic Gene Signature From the Immune Cell Infiltration Landscape of Osteosarcoma. Front Cell Dev Biol 2021;9:718624.
49. Zhang J, Yin J, Luo L, et al. Integrative Analysis of DNA Methylation and Transcriptome Identifies a Predictive Epigenetic Signature Associated With Immune Infiltration in Gliomas. Front Cell Dev Biol 2021;9:670854.
50. Zha C, Meng X, Li L, et al. Neutrophil extracellular traps mediate the crosstalk between glioma progression and the tumor microenvironment via the HMGB1/RAGE/IL-8 axis. Cancer Biol Med 2020;17:154-68.
51. Dermani FK, Samadi P, Rahmani G, et al. PD-1/PD-L1 immune checkpoint: Potential target for cancer therapy. J Cell Physiol 2019;234:1313-25.
52. Li B, Chan HL, Chen P. Immune Checkpoint Inhibitors: Basics and Challenges. Curr Med Chem 2019;26:3009-25.
53. Pardoll DM. The blockade of immune checkpoints in cancer immunotherapy. Nat Rev Cancer 2012;12:252-64.
54. Geeleher P, Cox NJ, Huang RS. Clinical drug response can be predicted using baseline gene expression levels and in vitro drug sensitivity in cell lines. Genome Biol 2014;15:R47.

(English Language Editor: A. Kassem)

Cite this article as: Wang Y, Wen H, Sun D. *SLC2A1* plays a significant prognostic role in lung adenocarcinoma and is associated with tumor immunity based on bioinformatics analysis. Ann Transl Med 2022;10(9):519. doi: 10.21037/atm-22-1430

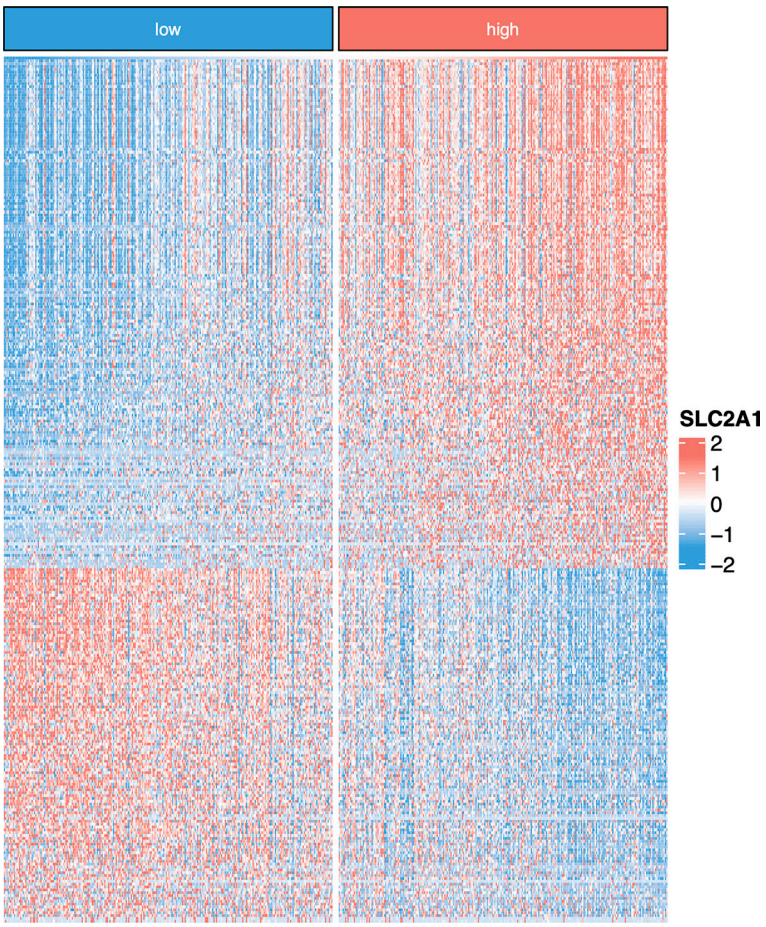

Figure S1 Expression heatmap of 306 differentially expressed genes were drawn using TCGA-LUAD. TCGA, The Cancer Genome Atlas; LUAD, lung adenocarcinoma.

https://dx.doi.org/10.21037/atm-22-1430

Table S1 Results of differential expression gene analysis of SLC2A1 high and low expression groups (adj.p<0.05, abs(logFC) >1)

	logFC	AveExpr	t	P value	adj.P.Val	B
SLC2A1	2.41875732	6.413888651	31.29571883	3.92E−121	6.84E−117	264.4237587
ANLN	1.643582815	4.381733454	16.62056414	5.84E−50	5.09E−46	102.752113
CTSV	1.557306557	2.328196711	15.66818299	1.63E−45	9.50E−42	92.62933008
KIF2C	1.434410993	4.195881295	15.20609788	2.18E−43	9.50E−40	87.79166506
RAD51	1.038381704	2.991386485	14.99844778	1.93E−42	6.74E−39	85.63523808
RRM2	1.432942225	4.912089775	14.97204899	2.55E−42	6.91E−39	85.36190228
CDCA8	1.263762859	4.594915324	14.96393586	2.77E−42	6.91E−39	85.27793553
CCNA2	1.315557801	4.41020325	14.92384547	4.22E−42	9.19E−39	84.86328007
PRR11	1.301445037	3.715774625	14.86296911	7.97E−42	1.39E−38	84.23446592
PLK1	1.254906092	4.079625998	14.76267398	2.27E−41	3.59E−38	83.20069397
ERO1A	1.048752091	6.560426216	14.73846714	2.92E−41	4.24E−38	82.95160424
KIF4A	1.40235115	3.684082595	14.65756763	6.77E−41	9.07E−38	82.12033615
SGO1	1.033250923	2.194709514	14.5637615	1.79E−40	2.08E−37	81.15877501
TPX2	1.550243441	5.361086449	14.54215274	2.24E−40	2.44E−37	80.93763228
CDC20	1.470393061	5.528112309	14.41644889	8.21E−40	8.41E−37	79.65388629
KIF23	1.190679278	3.237867977	14.32533716	2.10E−39	2.03E−36	78.72633146
CDC6	1.280609469	3.692222399	14.17091572	1.02E−38	8.49E−36	77.15998719
CKAP2L	1.15748135	2.77809617	13.96082123	8.74E−38	6.62E−35	75.04081695
FAM83D	1.282799138	4.156491674	13.95528502	9.24E−38	6.71E−35	74.98516389
MAD2L1	1.12442721	3.438925856	13.93611692	1.12E−37	7.83E−35	74.79255111
CIP2A	1.050453711	2.824668906	13.91249019	1.43E−37	9.26E−35	74.55529831
DLGAP5	1.327087026	3.721057761	13.91209178	1.43E−37	9.26E−35	74.55129913
CCNB2	1.211320787	4.418254706	13.82631765	3.42E−37	2.13E−34	73.69151312
CDCA5	1.279066869	4.122595882	13.81227221	3.95E−37	2.33E−34	73.55095302
BUB1B	1.196155399	3.41546521	13.80740213	4.14E−37	2.33E−34	73.50223067
PRC1	1.119769346	4.245203445	13.80724097	4.15E−37	2.33E−34	73.5006185
CEP55	1.294519985	4.370069256	13.75940128	6.74E−37	3.67E−34	73.02242833
HJURP	1.338274696	3.58782466	13.73247244	8.84E−37	4.67E−34	72.75358988
SKA3	1.108180272	2.952844503	13.72394197	9.64E−37	4.94E−34	72.66847801
NCAPG	1.235641052	3.233090006	13.70254662	1.20E−36	5.96E−34	72.45511513
CENPA	1.320465155	3.248622434	13.62416412	2.63E−36	1.28E−33	71.67476727
TTK	1.204996414	2.863253994	13.59719611	3.46E−36	1.63E−33	71.40676393
ARNTL2	1.424087689	3.637853773	13.5816722	4.04E−36	1.85E−33	71.25260239
CACNA2D2	−2.09139861	3.98395416	−13.55029193	5.54E−36	2.41E−33	70.94122937
SLC16A3	1.117703706	6.017819645	13.5208542	7.44E−36	3.16E−33	70.64943867
CDC45	1.209703162	3.51818659	13.50849239	8.42E−36	3.49E−33	70.52699577
KIF11	1.105124177	4.102086707	13.4342981	1.77E−35	7.17E−33	69.79321989
CD109	1.402347234	3.376779729	13.4298896	1.85E−35	7.28E−33	69.74968052
C16orf89	−2.615157966	7.152983499	−13.42717888	1.90E−35	7.28E−33	69.72291215
CENPW	1.12488967	4.751589169	13.4259848	1.92E−35	7.28E−33	69.71112149
GTSE1	1.122622089	3.104734843	13.35979859	3.72E−35	1.38E−32	69.05836278
DEPDC1B	1.129635159	2.730455025	13.30215466	6.61E−35	2.40E−32	68.49111485
RAD54L	1.107914467	2.747033671	13.2931719	7.23E−35	2.47E−32	68.40282614
NCAPH	1.202576799	3.704344187	13.28782277	7.62E−35	2.55E−32	68.35026503
CCNB1	1.164043547	5.560307743	13.27076171	9.03E−35	2.97E−32	68.18268949
MYBL2	1.643377644	5.466936508	13.23869479	1.24E−34	4.01E−32	67.86800799
SKA1	1.136216305	2.713462885	13.22173867	1.47E−34	4.66E−32	67.7017628
DEPDC1	1.17640124	2.578492378	13.17142139	2.42E−34	7.27E−32	67.2090436
FOXM1	1.348377776	4.327424488	13.13787945	3.37E−34	9.80E−32	66.88110515
NDC80	1.171934888	3.35213328	13.12770995	3.73E−34	1.07E−31	66.7817597
PLOD2	1.374901799	5.31071265	13.12215203	3.94E−34	1.11E−31	66.72748061
ORC1	1.052833958	2.959140331	13.09237694	5.29E−34	1.46E−31	66.43688836
ECT2	1.023133688	4.899718094	13.07267636	6.42E−34	1.75E−31	66.24479882
TRIP13	1.281388666	4.126712101	13.06066982	7.23E−34	1.94E−31	66.12780015
ARHGAP11A	1.016163067	3.19962814	13.0166984	1.12E−33	2.86E−31	65.69977457
MELK	1.309402165	3.854716444	12.98884953	1.47E−33	3.71E−31	65.42906204
DSG2	1.102624311	6.62548306	12.98111273	1.58E−33	3.94E−31	65.35390594
BIRC5	1.37767476	4.839970783	12.96671616	1.82E−33	4.48E−31	65.21411607
CDK1	1.167458324	4.67386877	12.94223137	2.32E−33	5.61E−31	64.97654934
NUSAP1	1.061342338	5.020558712	12.89966659	3.52E−33	8.41E−31	64.56409899
CCNE1	1.207628151	3.3228564	12.89293141	3.76E−33	8.74E−31	64.4988985
ADGRF4	1.562403093	2.126375896	12.86520743	4.93E−33	1.13E−30	64.23069624
LYPD3	1.736370307	3.663065075	12.82920724	7.02E−33	1.55E−30	63.8828684
SFTA3	−1.924146921	6.119286267	−12.77183129	1.23E−32	2.61E−30	63.32954258
TK1	1.163183709	6.577592567	12.70571052	2.34E−32	4.74E−30	62.69346685
HMGA1	1.089446724	8.378692404	12.70288068	2.41E−32	4.82E−30	62.66628214
KIF18B	1.24578078	3.109160659	12.70171359	2.43E−32	4.82E−30	62.65507145
CDKN3	1.209109619	3.841148117	12.69760482	2.53E−32	4.93E−30	62.6156083
EXO1	1.121871973	2.881892382	12.69701219	2.55E−32	4.93E−30	62.60991679
SPHK1	1.100870758	3.466653619	12.68669234	2.82E−32	5.39E−30	62.51083003
BUB1	1.120500045	3.641221981	12.65960423	3.66E−32	6.87E−30	62.25094089
ASF1B	1.013532587	4.730801738	12.63222791	4.78E−32	8.86E−30	61.98858051
PKMYT1	1.04503275	3.015432072	12.60960428	5.95E−32	1.07E−29	61.77199139
MCM10	1.107559318	2.509256939	12.60123284	6.45E−32	1.15E−29	61.69189826
UBE2C	1.573681466	6.119660395	12.55447177	1.01E−31	1.77E−29	61.24502883
UHRF1	1.073747942	3.316879696	12.52954408	1.29E−31	2.18E−29	61.00716631
NEK2	1.230733876	3.862793558	12.50845524	1.58E−31	2.65E−29	60.80612961
MKI67	1.244214422	4.12558227	12.40429103	4.31E−31	6.96E−29	59.81578914
TOP2A	1.310139574	5.678550302	12.37110289	5.93E−31	9.49E−29	59.50118328
LAMC2	1.554156064	6.591490883	12.35399178	6.99E−31	1.09E−28	59.33915595
FOSL1	1.618429068	3.707364727	12.35235846	7.10E−31	1.10E−28	59.32369618
CLSPN	1.009721994	2.325198476	12.3248054	9.25E−31	1.40E−28	59.06306514
SELENBP1	−1.427473232	7.123169401	−12.3039496	1.13E−30	1.70E−28	58.86599422
IQGAP3	1.127714744	3.845456329	12.27151757	1.54E−30	2.24E−28	58.55989618
KIFC1	1.160929417	4.491427642	12.22949031	2.30E−30	3.31E−28	58.16389038
GJB3	1.924515851	2.996341498	12.22019183	2.51E−30	3.59E−28	58.07637458
RAD51AP1	1.012975082	3.606441408	12.1845669	3.53E−30	4.96E−28	57.74141553
GGTLC1	−2.206383318	3.939045419	−12.11226158	7.01E−30	9.62E−28	57.06322544
HTR1D	1.301881052	1.699135642	12.05319447	1.23E−29	1.63E−27	56.51085906
HMMR	1.057248444	3.561346256	12.02198541	1.65E−29	2.14E−27	56.2196131
ESPL1	1.044486745	2.547925474	12.02078708	1.67E−29	2.15E−27	56.20843862
PFKP	1.103493148	6.644317155	11.99890227	2.05E−29	2.61E−27	56.00446996
ESYT3	−1.100250477	2.608743728	−11.9786705	2.48E−29	3.09E−27	55.81609255
SFTPB	−2.688597769	11.41586009	−11.94056478	3.55E−29	4.36E−27	55.46177541
KIF20A	1.032753207	3.969076093	11.92449918	4.13E−29	5.03E−27	55.31258331
MELTF	1.295252809	2.940899963	11.8353326	9.53E−29	1.13E−26	54.48660733
ADGRD1	−1.265132398	2.788065051	−11.82347536	1.07E−28	1.24E−26	54.37703516
TROAP	1.186108344	3.368453614	11.64819845	5.46E−28	5.91E−26	52.76465386
B3GNT8	−1.29830506	4.726249997	−11.50841692	1.99E−27	2.03E−25	51.48880499
SAPCD2	1.063997392	3.738603413	11.44136773	3.69E−27	3.69E−25	50.880023
ASPM	1.021208715	2.699134498	11.43289052	3.99E−27	3.97E−25	50.80320248
ADM	1.284999619	4.38988167	11.43003171	4.09E−27	4.05E−25	50.77730353
HILPDA	1.068672768	5.109332238	11.42095892	4.45E−27	4.38E−25	50.69513538
SPAG5	1.028641509	4.156215448	11.36233762	7.61E−27	7.36E−25	50.16516168
TDRD10	−1.322993845	2.4089497	−11.35681766	8.00E−27	7.66E−25	50.11534124
SLC16A1	1.255283873	3.529111711	11.35235397	8.34E−27	7.94E−25	50.07506477
PGC	−3.496426123	6.034464634	−11.34660243	8.79E−27	8.32E−25	50.02318171

Table S1 (*continued*)

https://dx.doi.org/10.21037/atm-22-1430

Table S1 (*continued*)

	logFC	AveExpr	t	P value	adj.P.Val	B
SHE	−1.298918068	3.200967784	−11.33512016	9.76E−27	9.14E−25	49.91965027
PLA2G4F	−1.221419959	2.658041297	−11.28531611	1.54E−26	1.42E−24	49.47131091
EGLN3	1.449615969	4.244120297	11.25813959	1.97E−26	1.81E−24	49.22716527
RND3	1.048063722	4.828998106	11.23186275	2.50E−26	2.26E−24	48.9914388
PLA2G1B	−1.819439163	3.05410419	−11.18155608	3.95E−26	3.53E−24	48.54107112
PKP2	1.365654581	2.717164	11.16182787	4.72E−26	4.19E−24	48.36478948
PIMREG	1.031981276	2.85900652	11.0956346	8.59E−26	7.34E−24	47.77470195
IGF2BP2	1.273563602	3.893089538	10.97119038	2.63E−25	2.10E−23	46.67115149
LOXL2	1.137116703	4.70298625	10.92113958	4.11E−25	3.16E−23	46.22947461
HLF	−1.354438367	2.906106758	−10.84944097	7.80E−25	5.83E−23	45.59895187
PTPRH	1.430598354	3.115052207	10.78608611	1.37E−24	1.01E−22	45.04396467
SLC22A31	−1.841355086	6.324039477	−10.75932169	1.74E−24	1.28E−22	44.81012196
INMT	−1.336680226	4.125991633	−10.69409123	3.09E−24	2.18E−22	44.24173352
KLF15	−1.159021647	2.905691884	−10.67905404	3.53E−24	2.47E−22	44.11101644
CENPF	1.077645972	3.744122838	10.67262512	3.73E−24	2.60E−22	44.05516598
SCTR	−1.717667756	3.406513464	−10.67085128	3.79E−24	2.63E−22	44.03975966
STEAP1	1.310995732	5.119809471	10.66005975	4.17E−24	2.88E−22	43.94606741
SUSD2	−1.831990152	5.623460191	−10.65330777	4.43E−24	3.05E−22	43.88747715
CRYBG2	1.087090963	2.010307341	10.64406459	4.80E−24	3.29E−22	43.8073078
TFAP2A	1.105545664	2.565007195	10.63608439	5.15E−24	3.52E−22	43.7381284
NUF2	1.052072219	3.477221549	10.62952387	5.46E−24	3.71E−22	43.68128068
AURKB	1.095246433	4.14958033	10.61339748	6.29E−24	4.21E−22	43.54163855
NAPSA	−2.17610569	9.481710777	−10.57883088	8.51E−24	5.62E−22	43.24277448
KRT16	1.758177079	2.58601824	10.53454475	1.25E−23	8.10E−22	42.86078706
RPL39L	1.141052495	5.232772471	10.52947501	1.31E−23	8.43E−22	42.81712394
CYP4B1	−2.05845892	5.064448888	−10.52589506	1.35E−23	8.64E−22	42.78629975
ADH1B	−1.703903269	3.538423616	−10.50003683	1.70E−23	1.07E−21	42.56385462
PBK	1.117711901	3.600717811	10.48022513	2.02E−23	1.26E−21	42.39366312
TMEM163	−1.225765635	3.783736834	−10.45848528	2.43E−23	1.52E−21	42.20714666
CFAP221	−1.100975958	2.331413985	−10.41469125	3.56E−23	2.19E−21	41.83217802
SCGB3A2	−2.742221472	7.431394418	−10.4024993	3.96E−23	2.40E−21	41.72797096
STC1	1.189138934	4.172116162	10.32523851	7.73E−23	4.60E−21	41.0694555
NKX2-1	−1.553282564	7.030166953	−10.2601957	1.35E−22	7.83E−21	40.51756767
GJB2	1.475777325	4.835652151	10.24900029	1.49E−22	8.57E−21	40.42280567
TMPRSS2	−1.285600679	5.560815562	−10.1910805	2.45E−22	1.38E−20	39.93364126
PRDM16	−1.129824197	2.215635447	−10.17103786	2.90E−22	1.63E−20	39.76479682
ADGRF5	−1.314925575	6.381966921	−10.14660288	3.58E−22	1.98E−20	39.55924816
SLC6A8	1.053625507	4.41980932	10.14075089	3.76E−22	2.08E−20	39.51006951
IGF2BP3	1.287478699	1.940468063	10.11240695	4.79E−22	2.63E−20	39.27214116
CLEC3B	−1.109527779	4.28347107	−10.08840478	5.88E−22	3.19E−20	39.07100568
C15orf48	1.453957943	6.374478351	10.08160332	6.22E−22	3.37E−20	39.01406817
GPR87	1.884337924	3.029606834	10.06815612	6.98E−22	3.75E−20	38.90157216
CTSH	−1.111645411	7.812089045	−10.05140928	8.04E−22	4.27E−20	38.76161244
NEIL3	1.007387843	2.223458062	10.02790922	9.82E−22	5.18E−20	38.5654765
ST3GAL5	−1.030495695	5.410554052	−9.996596163	1.28E−21	6.58E−20	38.30461027
DLC1	−1.03449182	4.311448991	−9.984407991	1.42E−21	7.23E−20	38.20321991
TMEM158	1.001084716	2.6962385	9.963553763	1.69E−21	8.52E−20	38.02993187
CRYM	−1.591867277	3.506320474	−9.905600497	2.75E−21	1.35E−19	37.54965378
TGFBI	1.094915664	6.570425232	9.883809312	3.31E−21	1.60E−19	37.36955341
PARM1	−1.173884263	6.574611247	−9.877845758	3.48E−21	1.67E−19	37.32031254
FSCN1	1.098387851	6.299273114	9.835325467	4.96E−21	2.36E−19	36.96980914
RHOV	1.460314759	4.825022652	9.811097448	6.08E−21	2.81E−19	36.77055306
ATOH8	−1.338748744	3.446625037	−9.807205464	6.28E−21	2.88E−19	36.73857584
SCNN1B	−1.368098211	5.183626443	−9.77982497	7.89E−21	3.55E−19	36.51385787
C7	−1.528403409	4.965211651	−9.766647636	8.80E−21	3.93E−19	36.4058616
MFSD2A	−1.01563597	4.933871516	−9.75794798	9.46E−21	4.22E−19	36.33461726
AK4	1.117090545	3.304780744	9.755496456	9.66E−21	4.29E−19	36.31454878
PMAIP1	1.054333715	4.661046291	9.743705388	1.07E−20	4.71E−19	36.21807391
CXCL17	−1.571665524	8.865630561	−9.740327764	1.10E−20	4.83E−19	36.19045284
HOPX	−1.446660464	6.413129899	−9.701215517	1.52E−20	6.60E−19	35.87108516
PLAU	1.286455491	7.021448588	9.682764377	1.77E−20	7.64E−19	35.72073089
VEGFD	−1.243679596	2.280758986	−9.537726825	5.83E−20	2.36E−18	34.54575559
RNASE1	−1.14413852	9.772676979	−9.468292335	1.03E−19	4.02E−18	33.9876272
COL7A1	1.148562451	2.52142411	9.418511932	1.54E−19	5.91E−18	33.58924182
AHNAK2	1.25232979	3.764616688	9.383972326	2.04E−19	7.72E−18	33.31369461
SLCO4A1	1.07063286	2.918278789	9.300244248	4.01E−19	1.46E−17	32.64870573
PCDH7	1.071573964	2.623711891	9.287815143	4.43E−19	1.61E−17	32.55035089
CHIA	−1.386478408	2.05383847	−9.242068803	6.40E−19	2.28E−17	32.18915381
ABCA3	−1.357672679	6.103729486	−9.240340384	6.48E−19	2.31E−17	32.17553173
SLC26A9	−1.583957807	3.922494146	−9.238575252	6.58E−19	2.34E−17	32.16162217
PEBP4	−1.756983763	4.226192603	−9.233993189	6.82E−19	2.40E−17	32.12552354
GGH	1.008338616	4.48374935	9.201390713	8.86E−19	3.05E−17	31.86904232
C4BPA	−1.832468689	6.950262105	−9.198900452	9.03E−19	3.11E−17	31.84947828
CIT	−1.212195628	4.481548094	−9.180384863	1.05E−18	3.57E−17	31.70413453
GREM1	1.245591438	3.173219094	9.166859444	1.17E−18	3.96E−17	31.59809522
PLPP4	1.025753542	1.921114699	9.126777961	1.61E−18	5.35E−17	31.28451523
TNS4	1.593685294	3.245684322	9.044574417	3.08E−18	9.86E−17	30.64448816
LPL	−1.290382215	4.522528517	−9.012096637	3.98E−18	1.25E−16	30.39277387
AQP3	−1.403670962	8.466210595	−8.98846991	4.79E−18	1.48E−16	30.21007101
WIF1	−1.794495625	3.237719133	−8.983004797	5.00E−18	1.54E−16	30.16785949
CDH3	1.304145486	5.420630986	8.934758383	7.30E−18	2.19E−16	29.79602364
MMP12	1.557684145	4.801041311	8.906520528	9.10E−18	2.70E−16	29.57907146
SFTA2	−1.509094321	8.799968914	−8.90064235	9.53E−18	2.80E−16	29.53397234
ZDHHC11B	−1.087432701	2.342230387	−8.892948164	1.01E−17	2.95E−16	29.47497316
SPOCK1	1.170449913	2.344321428	8.890617402	1.03E−17	3.00E−16	29.45710819
HABP2	−1.552678856	3.440952046	−8.886538343	1.06E−17	3.10E−16	29.42585102
SERPINB5	1.592830248	2.083834225	8.847910151	1.44E−17	4.11E−16	29.13037029
SCGB3A1	−2.395638237	7.123912243	−8.846022873	1.46E−17	4.17E−16	29.11595801
FMO5	−1.168109793	4.525303465	−8.831286479	1.63E−17	4.62E−16	29.00350055
KLK6	1.591054882	1.688165957	8.823045698	1.74E−17	4.90E−16	28.94067294
SLC22A3	−1.245301028	4.461326418	−8.816241159	1.84E−17	5.16E−16	28.88882771
PLA2G10	−1.288679601	3.10271615	−8.775446064	2.52E−17	6.98E−16	28.57861881
KRT6A	2.096666373	3.124476748	8.7415081	3.27E−17	8.90E−16	28.32136087
COL11A1	1.556361908	3.448011391	8.71772351	3.93E−17	1.05E−15	28.1415072
RAP1GAP	−1.13359257	5.318839202	−8.71238392	4.10E−17	1.10E−15	28.1011803
SLC46A2	−1.117900268	2.265298761	−8.695004795	4.68E−17	1.24E−15	27.97005239
CHRDL1	−1.164244236	3.48078303	−8.694487527	4.70E−17	1.24E−15	27.9661525
TMED6	−1.026610493	2.314846072	−8.668001011	5.76E−17	1.51E−15	27.76669059
IL20RB	1.289371153	2.465524845	8.607612117	9.14E−17	2.31E−15	27.31361357
PLPPR1	−1.05491044	2.02728324	−8.593721982	1.02E−16	2.55E−15	27.20973482
SCUBE2	−1.066306887	2.690177589	−8.584631084	1.09E−16	2.71E−15	27.14181549
GCLC	1.157495389	4.698772504	8.518402401	1.80E−16	4.35E−15	26.64863666
HMGA2	1.120800018	1.136651528	8.502313521	2.03E−16	4.88E−15	26.52926177
SFTPD	−1.766431156	7.609368673	−8.486472629	2.29E−16	5.47E−15	26.41189263
VSIG2	−1.460190665	4.826302744	−8.44195717	3.20E−16	7.45E−15	26.08294914
DSP	1.11963878	6.53677521	8.428851521	3.53E−16	8.15E−15	25.98635465
TFCP2L1	−1.057229443	4.261911989	−8.404372397	4.24E−16	9.75E−15	25.80623636

Table S1 (*continued*)

https://dx.doi.org/10.21037/atm-22-1430

Table S1 (*continued*)

	logFC	AveExpr	t	P value	adj.P.Val	B
PIGR	−1.998634334	7.588420622	−8.377513623	5.19E−16	1.18E−14	25.60906474
NR0B2	−1.417110097	2.444796979	−8.362728544	5.79E−16	1.30E−14	25.50073088
SORCS2	−1.058729655	3.138004783	−8.361616498	5.84E−16	1.31E−14	25.49258851
HSD17B6	−1.151913101	4.252797064	−8.349851198	6.38E−16	1.42E−14	25.40649375
CXCL8	1.17099245	5.543976445	8.349115913	6.41E−16	1.43E−14	25.40111622
CLIC6	−1.388223162	6.268353482	−8.261430229	1.23E−15	2.65E−14	24.76241029
GFRA3	−1.664001481	3.457418492	−8.231577003	1.53E−15	3.27E−14	24.54613294
LMO3	−1.209438065	4.687034782	−8.174679556	2.33E−15	4.82E−14	24.13559014
LRRK2	−1.210126497	3.808940036	−8.162735981	2.54E−15	5.22E−14	24.04968906
ANGPTL4	1.235672264	5.344354295	8.160059718	2.59E−15	5.31E−14	24.03045397
IRX2	−1.449358524	4.027720409	−8.158934898	2.62E−15	5.34E−14	24.02237101
KRT6B	1.178023072	1.202283103	8.155470131	2.68E−15	5.47E−14	23.99747855
CLDN2	−1.76138484	3.201706265	−8.115540679	3.59E−15	7.20E−14	23.71119491
GKN2	−1.544818316	2.447355601	−8.113303235	3.65E−15	7.31E−14	23.69518507
KIF12	−1.118720642	3.321953093	−8.087772495	4.40E−15	8.65E−14	23.51274328
TMPRSS11E	1.529034583	2.858291282	8.076038064	4.79E−15	9.36E−14	23.42903845
ARL14	1.169386107	1.369185522	8.070017611	5.01E−15	9.73E−14	23.38612943
FOLR1	−1.485228812	7.325921274	−8.048536676	5.85E−15	1.13E−13	23.23323212
TNNT1	1.553206176	3.738863594	7.989574186	8.96E−15	1.67E−13	22.81517273
C9orf152	−1.04427476	4.364813716	−7.959109391	1.12E−14	2.07E−13	22.60010576
FOXA2	−1.276658047	4.556897115	−7.916394561	1.52E−14	2.76E−13	22.29963805
ATP13A4	−1.226573356	3.650370152	−7.878280872	1.99E−14	3.58E−13	22.03260269
DACT2	−1.19302641	2.106929735	−7.858762339	2.29E−14	4.07E−13	21.89624097
ALOX15B	−1.303072338	5.221582902	−7.856320864	2.33E−14	4.14E−13	21.87920283
CPB2	−1.233010224	2.064653565	−7.779412784	4.02E−14	6.93E−13	21.34461951
SLC14A2	−1.070842116	0.912049685	−7.774418622	4.17E−14	7.15E−13	21.31004849
POPDC3	1.019810625	1.320724147	7.773784405	4.18E−14	7.16E−13	21.30565951
GJB1	−1.512661309	3.713397238	−7.755590408	4.76E−14	8.08E−13	21.17987161
SFTPA1	−2.200729555	9.67411427	−7.679143459	8.14E−14	1.33E−12	20.65388643
ACKR1	−1.015687237	3.824892203	−7.586387693	1.55E−13	2.44E−12	20.0212444
C1orf116	−1.117227983	6.603534881	−7.581965973	1.60E−13	2.50E−12	19.99123883
SFTPA2	−2.105174101	9.970342895	−7.500388605	2.81E−13	4.18E−12	19.44016744
COL12A1	1.035155633	4.518018527	7.473302378	3.39E−13	5.00E−12	19.25825039
ADRA2A	−1.053467328	3.041657713	−7.468771505	3.50E−13	5.14E−12	19.2278716
ELAPOR1	−1.257010233	4.277484894	−7.418033511	4.95E−13	7.09E−12	18.888693
SFTPC	−2.455084982	6.69712124	−7.35680645	7.50E−13	1.05E−11	18.48187714
MMP11	1.169538068	4.899051766	7.296528849	1.13E−12	1.51E−11	18.0840336
GGT6	−1.154392135	3.105844117	−7.2901481	1.18E−12	1.57E−11	18.04207471
PRR15	1.169898657	3.193268766	7.273151913	1.32E−12	1.75E−11	17.93045557
CDA	1.251948575	4.671500064	7.20909118	2.02E−12	2.61E−11	17.51165361
KCNJ15	−1.010070736	3.519838161	−7.16042893	2.80E−12	3.54E−11	17.19553945
PRSS3	1.054650634	1.490277594	7.153235665	2.93E−12	3.71E−11	17.14895976
PITX1	1.06968853	3.182514418	7.14733356	3.05E−12	3.85E−11	17.11076951
FAM83A	1.157072171	5.408961385	7.14460651	3.11E−12	3.91E−11	17.09313253
MET	1.066158625	6.361581999	7.090150934	4.45E−12	5.44E−11	16.74209981
MYBPHL	−1.041909786	2.135034608	−7.067071743	5.18E−12	6.29E−11	16.59399106
PSCA	1.518334224	2.706190585	7.049051356	5.83E−12	7.02E−11	16.47862264
SPP1	1.202954773	8.760695143	7.013581604	7.35E−12	8.72E−11	16.25224975
KRT81	1.293594852	2.164075465	7.006265262	7.71E−12	9.12E−11	16.20567288
DKK1	1.354967758	2.791744618	6.993123303	8.40E−12	9.82E−11	16.12210998
AQP4	−1.345640572	4.406366178	−6.944691702	1.15E−11	1.32E−10	15.81527726
ALPL	−1.183808731	5.987056876	−6.861022524	1.97E−11	2.17E−10	15.28936344
DMBT1	−1.513088987	4.421743805	−6.824446483	2.49E−11	2.70E−10	15.06112355
FGFBP1	1.209001612	3.370879549	6.819670054	2.57E−11	2.78E−10	15.0313929
AQP5	−1.691978048	4.655097216	−6.746405703	4.09E−11	4.29E−10	14.57753892
MYEOV	1.212548521	2.75220973	6.744770465	4.14E−11	4.33E−10	14.56745576
PPP1R1B	−1.313086578	4.372884425	−6.714796399	5.00E−11	5.13E−10	14.38299285
EREG	1.30181554	2.211924743	6.700667312	5.46E−11	5.59E−10	14.29627989
TRIM29	1.127833311	2.313557405	6.679366311	6.25E−11	6.31E−10	14.16584101
PCP4L1	−1.273183916	4.464929779	−6.615055055	9.34E−11	9.16E−10	13.77414179
PLA2G12B	−1.027984841	2.242946285	−6.521576873	1.67E−10	1.57E−09	13.21049456
LY6K	1.073597956	2.204936655	6.502058592	1.88E−10	1.76E−09	13.09366068
AMBP	−1.081728856	2.119524683	−6.452600847	2.54E−10	2.33E−09	12.79894234
APOH	−1.142100738	2.826343944	−6.403392529	3.43E−10	3.08E−09	12.50760773
AGER	−1.171842787	5.431362625	−6.402149936	3.46E−10	3.10E−09	12.5002756
KRT17	1.290089187	5.408101234	6.357676681	4.53E−10	3.97E−09	12.238652
UPK1B	1.042968915	0.990074702	6.10836008	1.99E−09	1.58E−08	10.8009625
TMEM59L	−1.201760256	3.121491155	−6.074338635	2.42E−09	1.90E−08	10.60861973
SNCG	1.005020168	5.047061461	6.072380222	2.45E−09	1.92E−08	10.59757597
CXCL5	1.078377419	3.235960858	6.0551592	2.71E−09	2.10E−08	10.50059703
SLC34A2	−1.067411024	9.73670231	−6.053369511	2.74E−09	2.12E−08	10.4905322
PCSK2	−1.17023886	1.32529353	−6.028737731	3.16E−09	2.41E−08	10.35227027
CD207	−1.077443615	3.06987106	−5.884618746	7.20E−09	5.18E−08	9.553134318
MS4A15	−1.184184329	2.928059277	−5.876830254	7.53E−09	5.39E−08	9.510427288
MAGEA3	1.276041109	1.531525756	5.827742965	9.93E−09	6.94E−08	9.242402226
ORM1	−1.041362804	3.709192157	−5.742299059	1.60E−08	1.08E−07	8.780563153
FDCSP	−1.027898817	3.437419941	−5.729977965	1.71E−08	1.15E−07	8.714459584
SERPIND1	−1.014692994	2.506937146	−5.628584704	2.99E−08	1.91E−07	8.175227373
SPINK1	−1.532529636	5.888649234	−5.438177056	8.34E−08	4.89E−07	7.185638242
CRLF1	−1.269741912	4.845834761	−5.437897985	8.35E−08	4.90E−07	7.184210061
MMP1	1.098200543	5.696208434	5.428412718	8.78E−08	5.12E−07	7.135706719
PI3	1.016484961	3.330330823	5.4129825	9.53E−08	5.54E−07	7.056964798
TCN1	1.286444884	2.835186776	5.386124106	1.10E−07	6.31E−07	6.920380535
KLK11	−1.135509449	3.42506557	−5.315184761	1.59E−07	8.86E−07	6.562548325
CLDN18	−1.213514184	3.674673273	−5.212683769	2.70E−07	1.44E−06	6.0530237
AGR3	−1.01631729	6.472613351	−5.054528339	6.01E−07	3.01E−06	5.284378995
AKR1B10	1.389697019	3.241850683	4.927635941	1.12E−06	5.33E−06	4.683177398
GSTA1	−1.041916081	4.370870927	−4.721250887	3.03E−06	1.33E−05	3.73511012
SCGB1A1	−1.512787077	6.148281333	−4.614901894	4.97E−06	2.09E−05	3.2610859
ASCL1	−1.081434859	1.534932767	−4.609387208	5.10E−06	2.14E−05	3.23677624
CALCA	−1.253317578	1.924430309	−4.352556261	1.62E−05	6.19E−05	2.134381424
TFF1	1.193625933	3.308794365	4.003548931	7.16E−05	0.000239472	0.730703998

https://dx.doi.org/10.21037/atm-22-1430

Table S2 Results of GO enrichment analysis containing logFC for SLC2A1 related differential genes.

Ontology	ID	Description	setSize	enrichmentScore	NES	P value	p.adjust	qvalues	rank	leading_edge
CC	GO:0005576	Extracellular region	125	-0.292583838	-2.377642871	0.001490313	0.016661795	0.011692488	72	tags=36%, list=24%, signal=47%
CC	GO:0005615	Extracellular space	104	-0.338404417	-2.637076986	0.001517451	0.016661795	0.011692488	72	tags=40%, list=24%, signal=47%
MF	GO:0005488	Binding	276	0.358355609	2.222655997	0.002659574	0.016661795	0.011692488	140	tags=49%, list=46%, signal=273%
CC	GO:0005622	Intracellular anatomical structure	246	0.249840001	1.929538949	0.002898551	0.016661795	0.011692488	132	tags=48%, list=43%, signal=139%
CC	GO:0043228	Non-membrane-bounded organelle	110	0.351254306	3.064729333	0.002923977	0.016661795	0.011692488	178	tags=81%, list=58%, signal=53%
CC	GO:0043232	Intracellular non-membrane-bounded organelle	110	0.351254306	3.064729333	0.002923977	0.016661795	0.011692488	178	tags=81%, list=58%, signal=53%
BP	GO:0050794	Regulation of cellular process	195	0.2390881	2.136088519	0.002941176	0.016661795	0.011692488	140	tags=54%, list=46%, signal=81%
MF	GO:0005515	Protein binding	245	0.341020358	2.636977273	0.00295858	0.016661795	0.011692488	169	tags=62%, list=55%, signal=140%
CC	GO:0005634	Nucleus	121	0.29956241	2.708553234	0.00297619	0.016661795	0.011692488	177	tags=77%, list=58%, signal=54%
BP	GO:0016043	Cellular component organization	134	0.349091002	3.14216494	0.003215434	0.016661795	0.011692488	169	tags=75%, list=55%, signal=60%
BP	GO:0071840	Cellular component organization or biogenesis	134	0.349091002	3.14216494	0.003215434	0.016661795	0.011692488	169	tags=75%, list=55%, signal=60%
CC	GO:0005737	Cytoplasm	216	0.214867889	1.854808664	0.008928571	0.042410714	0.029761905	112	tags=43%, list=37%, signal=92%

Table S3 Results of KEGG enrichment analysis containing logFC for SLC2A1 related differential genes.

ID	Description	setSize	enrichmentScore	NES	P value	p.adjust	qvalues	rank	leading_edge
hsa04110	Cell cycle	16	0.506896552	2.266032203	0.001429971	0.005719886	0.003010466	159	tags=100%, list=52%, signal=51%
hsa04114	Oocyte meiosis	11	0.484745763	1.830681737	0.009039901	0.018079801	0.009515685	163	tags=100%, list=53%, signal=48%

Table S4 Results of GSEA enrichment analysis containing logFC for SLC2A1 related differential genes

ID	Description	setSize	enrichmentScore	NES	P value	p.adjust	qvalues	rank	leading_edge
HALLMARK_G2M_CHECKPOINT	HALLMARK_G2M_CHECKPOINT	35	0.551469393	3.387921132	4.00E-08	3.20E-07	4.21E-08	149	tags=97%, list=49%, signal=56%
HALLMARK_E2F_TARGETS	HALLMARK_E2F_TARGETS	30	0.448623465	2.541945996	7.17E-05	2.87E-04	3.77E-05	101	tags=70%, list=33%, signal=52%
HALLMARK_MITOTIC_SPINDLE	HALLMARK_MITOTIC_SPINDLE	22	0.485915493	2.466256924	1.86E-04	4.95E-04	6.52E-05	168	tags=100%, list=55%, signal=49%
HALLMARK_GLYCOLYSIS	HALLMARK_GLYCOLYSIS	18	0.493055556	2.332225144	9.62E-04	0.001923517	2.53E-04	164	tags=100%, list=54%, signal=49%
HALLMARK_MTORC1_SIGNALING	HALLMARK_MTORC1_SIGNALING	10	0.537546645	1.948032945	0.009670248	0.015472396	0.002035842	123	tags=90%, list=40%, signal=56%
HALLMARK_SPERMATOGENESIS	HALLMARK_SPERMATOGENESIS	10	0.525471687	1.904274105	0.012270596	0.016360794	0.002152736	118	tags=90%, list=39%, signal=57%
HALLMARK_EPITHELIAL_MESENCHYMAL_TRANSITION	HALLMARK_EPITHELIAL_MESENCHYMAL_TRANSITION	15	0.422654174	1.854485291	0.016337481	0.018671406	0.002456764	162	tags=93%, list=53%, signal=46%

https://dx.doi.org/10.21037/atm-22-1430

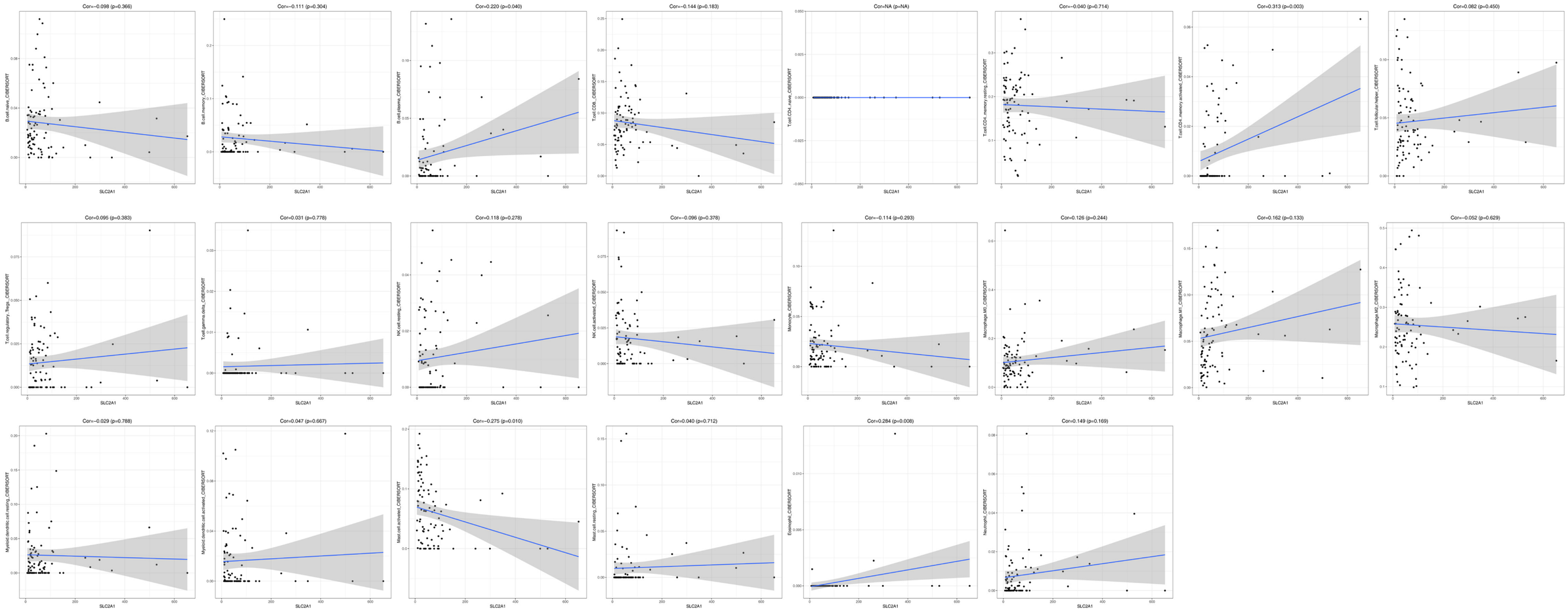

Figure S2 Results of the correlation analysis between SLC2A1 and 22 tumor immune infiltration cells by CIBERSORT using GSE40419.

https://dx.doi.org/10.21037/atm-22-1430

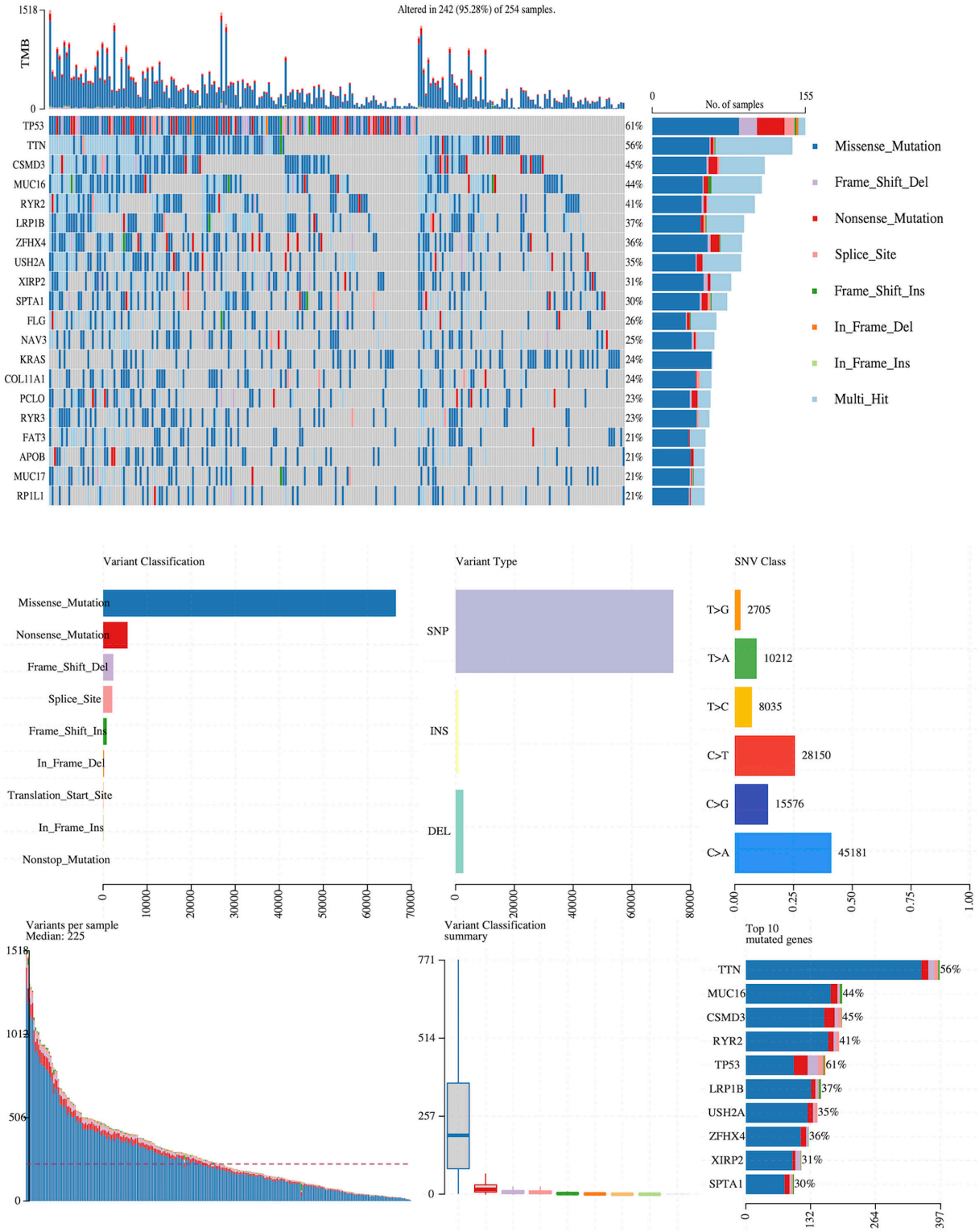

Figure S3 Waterfall plot of somatic mutations in patients with SLC2A1 overexpression in TCGA-LUAD. TCGA, The Cancer Genome Atlas; LUAD, lung adenocarcinoma.

https://dx.doi.org/10.21037/atm-22-1430

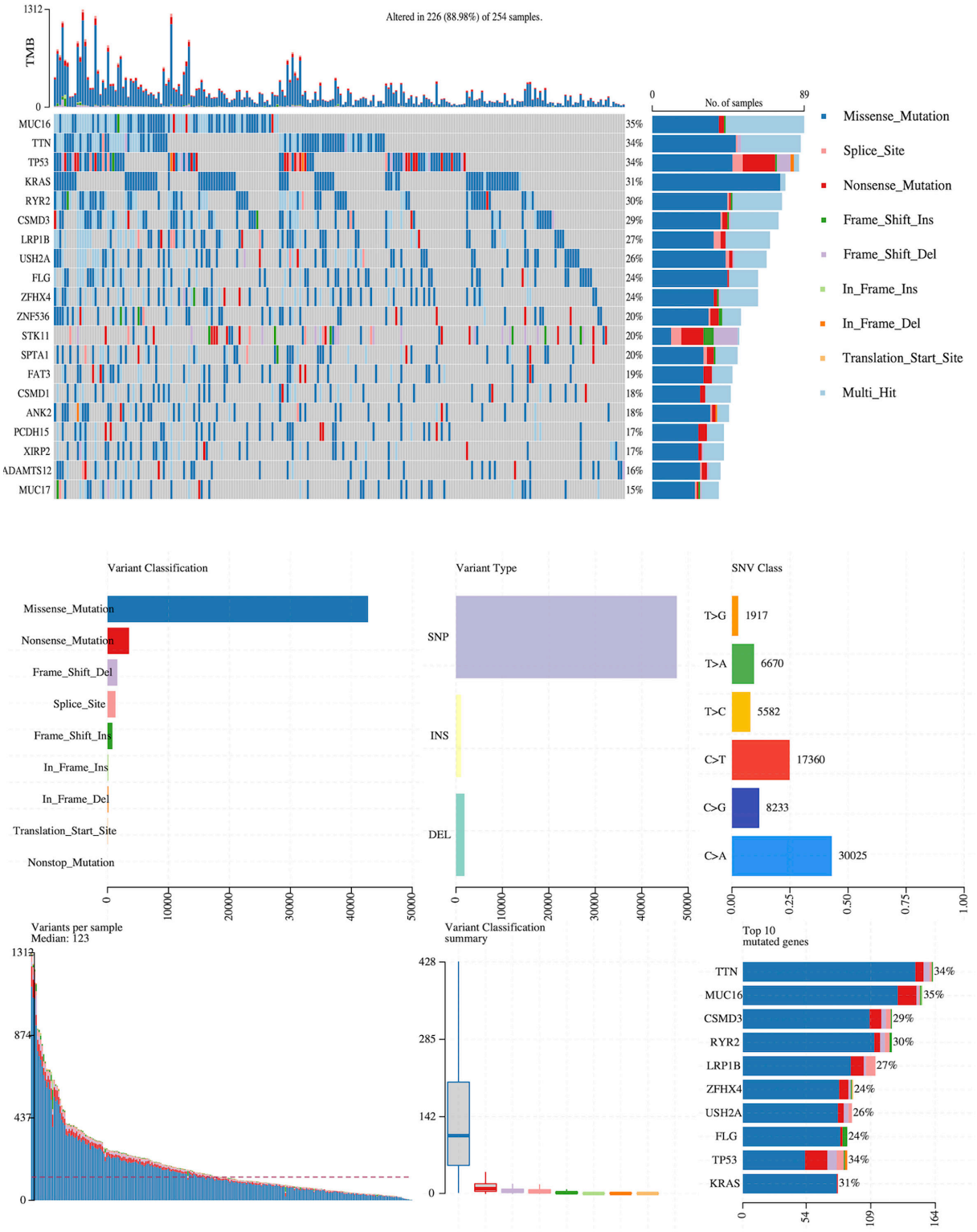

Figure S4 Waterfall plot of somatic mutations in patients with SLC2A1 low expression in TCGA-LUAD. TCGA, The Cancer Genome Atlas; LUAD, lung adenocarcinoma.

https://dx.doi.org/10.21037/atm-22-1430

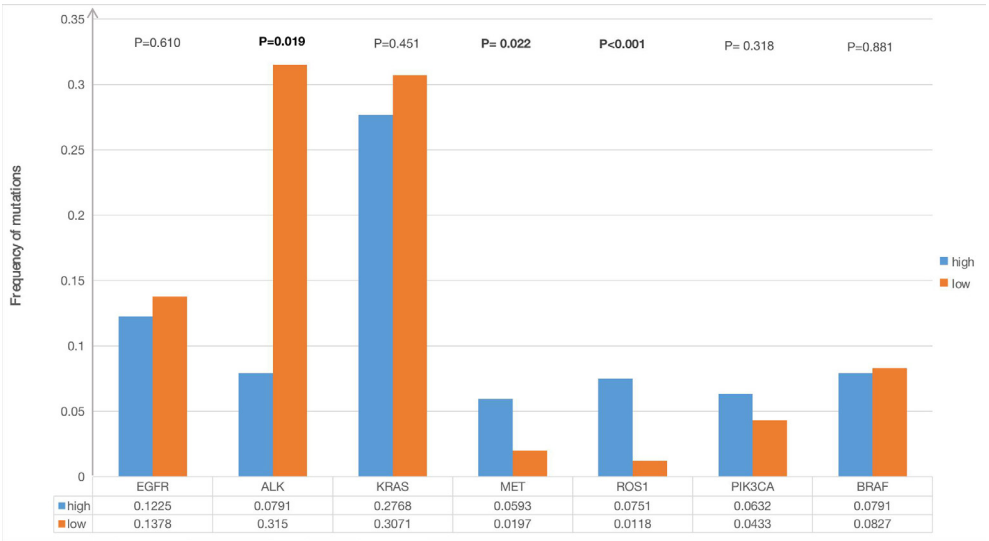

Figure S5 Mutation frequency of driver genes in SLC2A1 high and low expression groups.

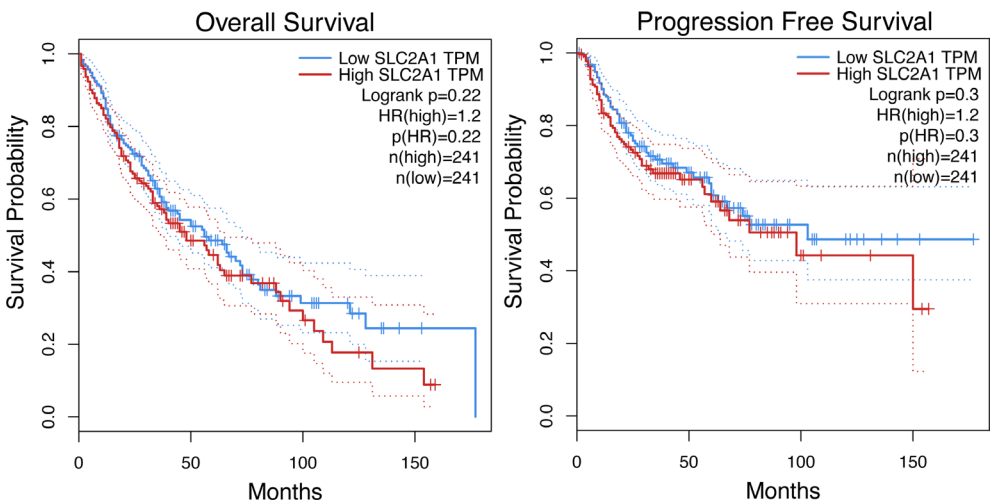

Figure S6 The survival curves of LUSC patients with high and low SLC2A1 expression in GEPIA. LUSC, lung squamous cell carcinoma; GEPIA, Gene Expression Profiling Interactive Analysis.

https://dx.doi.org/10.21037/atm-22-1430